Alma Mater Studiorum - Università di Bologna

SCUOLA DI SCIENZE

Dipartimento di Chimica Industriale"Toso Montanari"

Corso di Laurea Magistrale in

Chimica Industriale

Classe LM-71 - Scienze e Tecnologie della Chimica Industriale

Synthesis and dynamic study of atropisomeric compounds containing boron-carbon bond

Tesi di laurea sperimentale

CANDIDATO

Elia Mercanti

RELATORE

Prof. Dr. Andrea Mazzanti

CORRELATORE

Dr. Michele Mancinelli

Sessione III

Anno Accademico 2014-2015

"La mente è come un paracadute. Funziona solo se si apre"

Albert Einstein

INDEX

SOMMARIO

In questo lavoro di tesi è stato studiato il comportamento stereodinamico di diverse 1,2-azaborine sostituite sull'atomo di boro (**7a**, **7b**, **13**). A seconda dell'ingombro sterico generato dal sostituente arilico asimmetrico, le risultanti conformazioni possono essere stereolabili o configurazionalmente stabili. Attraverso analisi NMR dinamico e simulazione della forma di riga è possibile ricavare i valori dell'energia libera di rotazione dei differenti conformeri. Quando la barriera di rotazione è più alta di 22-23 kcal/mol si ottengono atropoisomeri stabili e fisicamente separabili come nel caso del composto **13** e l'energia di attivazione del processo rotazionale è determinabile attraverso analisi cinetica. La configurazione assoluta dei due atropoisomeri è stata assegnata mediante il metodo ECD. Il composto isosterico **21** è stato sintetizzato in modo da confrontare la barriera di rotazione del legame B-C$_{arilico}$ con quella del legame C$_{naftalenico}$-C$_{arilico}$.

ABSTRACT

In this thesis we studied the stereodynamic behavior of 1,2-azaborines variously substituted on boron (**7a**, **7b**, **13**). Depending on the hindrance of the asymmetric aryl substituent the resulting conformations could be stereolabile or configurationally stable. Through dynamic NMR and lineshape simulation, the energy rotational barriers of the different conformers are obtained. When the barrier is higher than 22-23 kcal/mol stable atropisomers that are fisically separable could be obtained (case of compound **13**) and the free activation energy barrier is determinable by kinetic analysis. Absolute configuration of two atropisomers were assigned by comparison between computational calculations and experimental ECD. Isosteric compound **21** is then synthesized in order to compare the rotational barrier around B-C$_{aryl}$ with the one around C$_{naphth}$-C$_{aryl}$ bond.

1. Introduction

Chirality is a property of asymmetry important in several branches of science. The word chirality is derived from the Greek, χειρ (kheir), "hand", a familiar chiral object.[1] In 1848, the compresence and significance of chirality was recognized by Louis Pasteur, one of the pioneering of the stereochemistry, which prompted his famous statement of chiral universe (*l'univers est dissymetrique*).[2] Today, is well renowned that chirality can indeed be encountered at all levels in nature in the form of the elementary particle known as the helical neutrino, DNA, carbohydrates and inherently chiral proteins. Pasteur realized that chiral objects exist as a pair of enantiomorphous mirror images that are not superimposable. At the molecular level, chirality gives rise to enantiomers that can exhibit strikingly different chemical and physical properties in a chiral environment.[3] The increasing demand for enantiopure chemicals has been accompanied by significant progress in asymmetric synthesis[4] and catalysis,[5] and by the development of analytical techniques for the determination of the stereochemical purity of chiral compounds.

A well renowned example of a chiral drug is thalidomide that undergoes enantioconversion under physiological conditions. This drug was prescribed to pregnant women in the 1960s to alleviate morning sickness. One of enantiomeric forms of thalidomide does indeed have sedative and antinausea effects, but the other enantiomer is a potent teratogen for the fetus.[6]
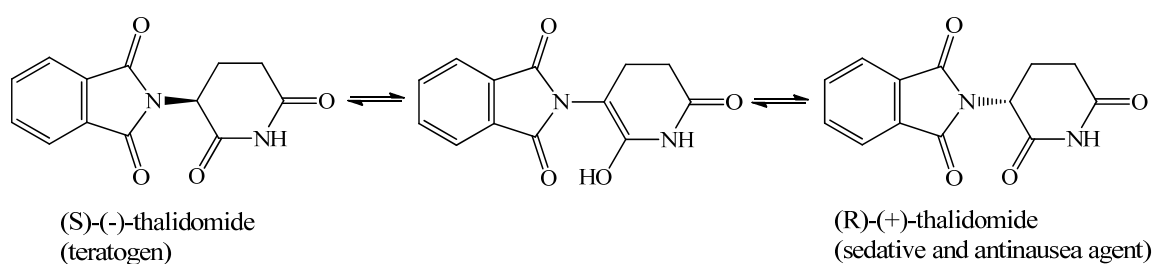

(S)-(-)-thalidomide
(teratogen)

(R)-(+)-thalidomide
(sedative and antinausea agent)

Figure 1. Interconversion of the enantiomers of thalidomide.

Since the thalidomide tragedy, the significance of the stereochemical integrity of biologically active compounds has received increasing attention and the investigation of the stereodynamic properties of chiral molecules has become an integral part of modern drug development.

1.1 Axial Chirality and Atropisomerism

Chirality is not an exclusive feature of molecules that show one or more "classic" stereogenic center at carbon atoms. In fact, many compounds exhibit optical properties due to the presence of axial chirality. As the molecules containing stereogenic center, compounds holding a set of substituents in a different spatial rearrangement, could be chiral. This, often overlooked, source of chirality is called atropisomerism (from the Greek, *a* = not *tropos* = turn), a term proposed by Kuhn in 1933.[7] Therefore, atropisomerism are enantiomeric or diastereomeric conformers that result from an hindered rotation around a single bond due to steric hindrance and/or electronics factors. Atropisomers are involved in a chemical equilibrium that is thermally dependent; they differ in this way from many other types of chiral structure because the intercoversion each other occur without breaking and reforming of covalent bonds.

In 1922, before the definition given by Kuhn, atropisomerism was experimentally detected for the first time in 6,6'-dinitro-2,2'-diphenic acid, by Christie and Kenner.[8]

In 1983, Oki proposed a boundary rule between atropisomers and conformers (and therefore between configuration and conformation) with his arbitrary definition that atropisomers are conformers which interconvert with a half-life ($t_{1/2}$) of at least 1000 s at +25 °C, corresponding to a racemization barrier of 21.8 kcal/mol.[9]

Given the absence of a stereogenic center, the absolute configuration of conformers is assigned using the concept of helicity based on a dihedral angle: a right-handed helix is described as *P* (plus), a left-handed one as *M* (minus) and the designations are based on the same Cahn-Ingold-Prelog priority rules used for tetrahedral stereocenters.
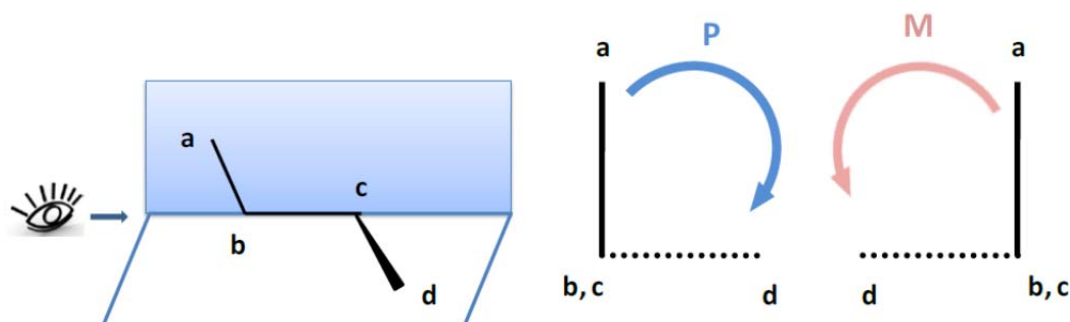
Scheme 1. Representation of dihedral angle and its nomenclature.

In the Scheme 1 is reported a chain of four atoms **a-b-c-d.** In this case, **a** and **d** represented the two "fiducial" groups (assigned with CIP priority rules) and **b** and **c** are the atoms linked by the bond that may generate axial chirality. The torsion angle is the dihedral between the plane containing the atoms **a**, **b**, **c** and that containing **b**, **c**, **d** (from -180° to +180°). If the bond **a-b** is rotated in clockwise direction in order to eclipse **c-d** the dihedral angle is considered to be positive and absolute configuration is *P*, instead, if the bond **a-b** is rotated in anticlockwise direction in order to eclipse **c-d** the dihedral angle is considered to be negative and absolute configuration is *M*.

It is important to note that sign of a dihedral angle remains the same regardless of the side from which it is observed, provided that the observation starts from the nearest atom and follows the chain toward the farthest.

The concept of axial chirality as a stereogenic source in a rotationally hindered compound was for many years relegated to the academic field. However this situation changed with the discovery of many bioactive natural compounds containing stereogenic chiral axes[10] and with the discovery of many catalysts useful for asymmetric synthesis.[11]

Some naturally occurring atropisomers have important biological activities. For instance, knipholone exhibits good antimalarial and antitumor activities[12] and gossypol inhibits sperm production and motility in a variety of male animals and in humans, but it does not affect sex hormone levels or libido[13] (Figure 2).
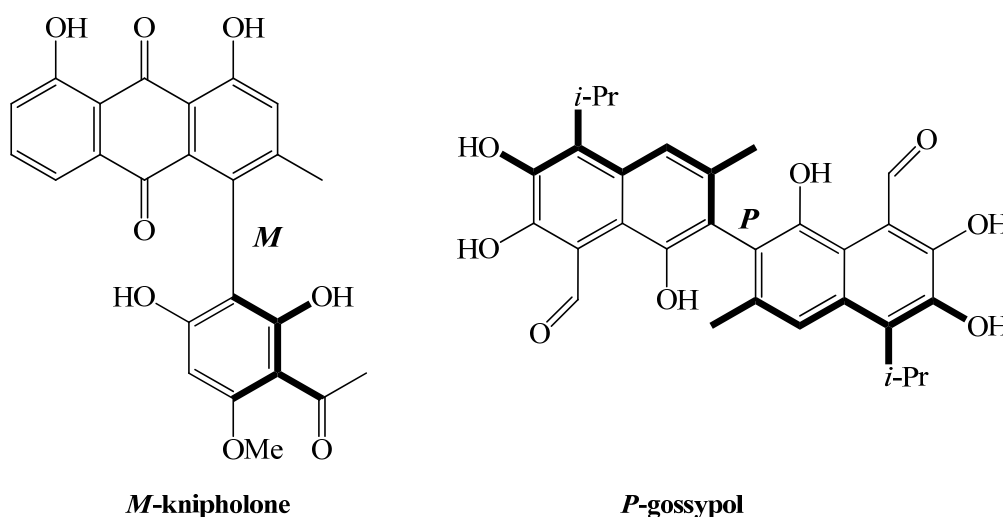

Figure 2. Examples of axial chirality in natural organic compounds.

1.2 Azaborines

Boron plays a crucial role in the field of chemistry.[14] Due to the boron unique electronic structure and ability to form covalent bonds with carbon, the inclusion of boron in organic structure has recently received significant attention in biomedical research.[15]

An emerging strategy of incorporation of boron in organic structures is the substitution of a C=C bond with an isoelectronic and isosteric B-N unit.

The isoelectronic nature between the B-N and C=C bonding arises from the fact that boron has three valence electrons and nitrogen has five electrons, and consequently, a BN unit has the same valence electron count as corresponding CC unit in which each carbon contributes four valence electrons.

The first example of BN/CC isosterism of an arene was reported by Alfred Stock in 1926 with the synthesis of borazine ($c\text{-}B_3N_3H_6$) the inorganic counterpart to the quintessential aromatic compound benzene ($c\text{-}C_6H_6$).[16]

Since the pioneering contribution of Stock, the isoelectronic relationship between B-N has led to the development of aromatic systems partially substituted with boron and nitrogen.

In 1958, Dewar reported the synthesis of the first singly BN-substituted aromatic compounds, 9,10-azaboraphenanthrenes.[17] The reaction of 2-phenylaniline with BCl_3 and $AlCl_3$ (Scheme 2) gave 9,10-azaboraphenanthrene **II**, presumably through the Friedel-Crafts cyclization of intermediate **I** and the substitution of various nucleophiles at the reactive B-Cl unit of **II** allowed for the synthesis of several BN-phenanthrene derivatives (**III-VI**).
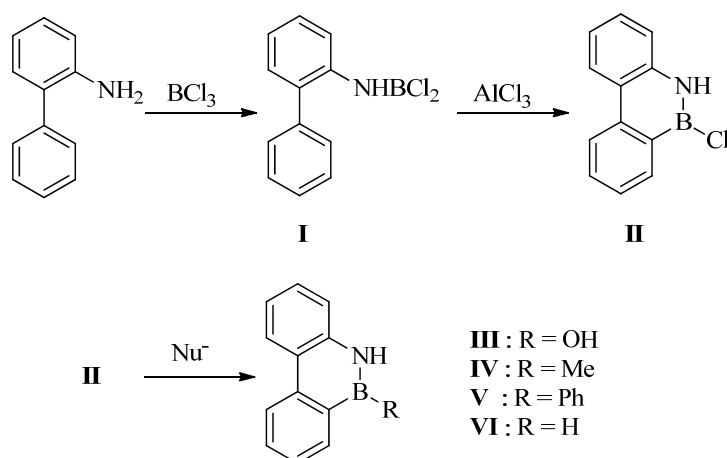
Scheme 2. Preparation of boron-substituted 9,10-borazaphenanthrene derivatives (III-VI).

One year later, in 1959, Dewar et al synthesized the first BN-naphthalene (Figure 3),[18] with the same synthetic procedure, whose reactivity and properties have attracted much attention over the past few years.[19]
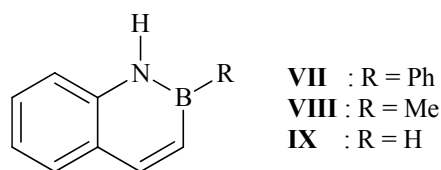

VII : R = Ph
VIII : R = Me
IX : R = H

Figure 3. Molecular scaffold of 1,2-azaboranphthalenes

Theoretical calculations as well as experimental data have shown that 1,2-azaborines are stable aromatic molecules whose aromaticity and thermal stability are slightly lower than those of the corresponding C=C aromatic systems.[20]

Azaborines have demonstrated antifungal activity against several different fungi in addition to exhibiting antibacterial activity against Gram-negative bacteria.[21] In the Figure 4 is shown one of the investigated molecule that inhibits bacteria's growth.
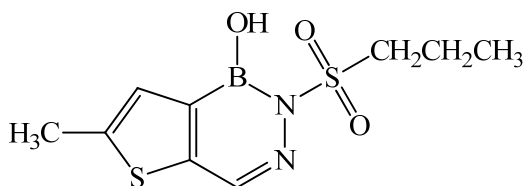

Figure 4. Example of diazaborines that inhibits the growth of some bacteria.

The molecular target of diazaborines has been identified as the NAD(P)H-dependent enoyl acyl carrier protein reductase (ENR), which catalyzes the last reductive step of fatty acid synthase. ENR from Mycobacterium tuberculosis is the target for the front-line antituberculosis drug isoniazid.

In addition to their medicinal chemistry applications, 1,2-azaborines have made a significant impact in materials science due to their photophysical properties.[22] Replacing one or more of the carbon atoms in polycyclic aromatic hydrocarbons (PAHs) with boron decreases the HOMO-LUMO gap material providing access to molecule with chemiluminescent properties. Azaborines have been shown to function as organic light-emitting diodes (OLEDs)[23] and organic field-effect transistors (OFETs).[24] For this reason the synthesis of functionalized 1,2-azaborines could provide access to new classes of chemiluminescent compounds as well. A molecule that has fascinating properties is reported in Figure 5.
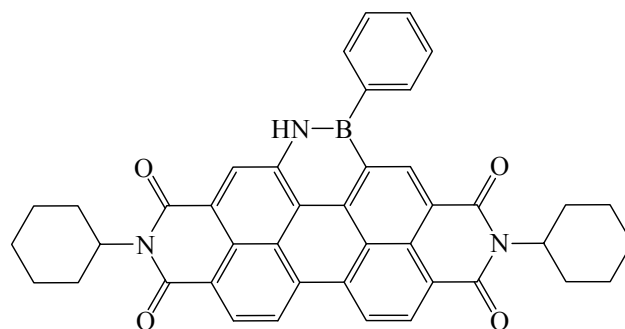
Figure 5. PDI-1BN structure

PDI-1BN consisting of azaborine and perlyene diimide, shows very good stability and displays high selectivity and sensitivity only to fluorine ion (Figure 6). [25]

Figure 6. Fluorescence spectrum of PDI-BN.

In fact, fluorescence spectrum of PDI-1BN shows emission bands in the range of 500-650 nm but upon the addiction of 10 eq of Bu_4NF, significant fluorescence quenching was observed which is attributed to the high charge of fluorine ion.

2. Aim of the thesis

The target of this project is to study the conformational behaviour of variously substituted 1,2-azaborines. Particular efforts have been made in order to obtain stable atropisomeric compounds with axial chirality on the boron-carbon axis.
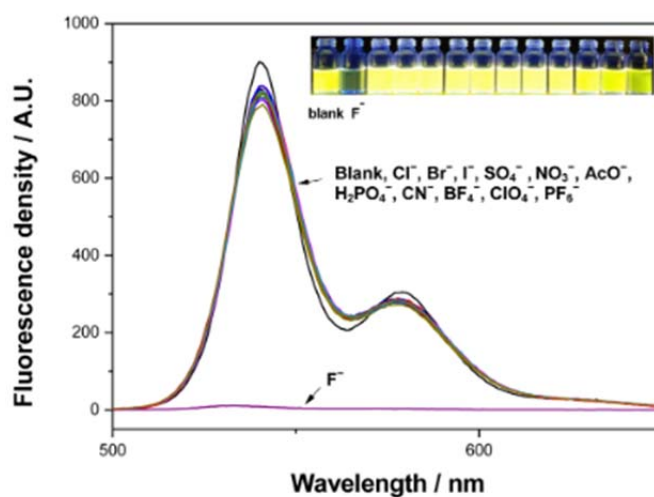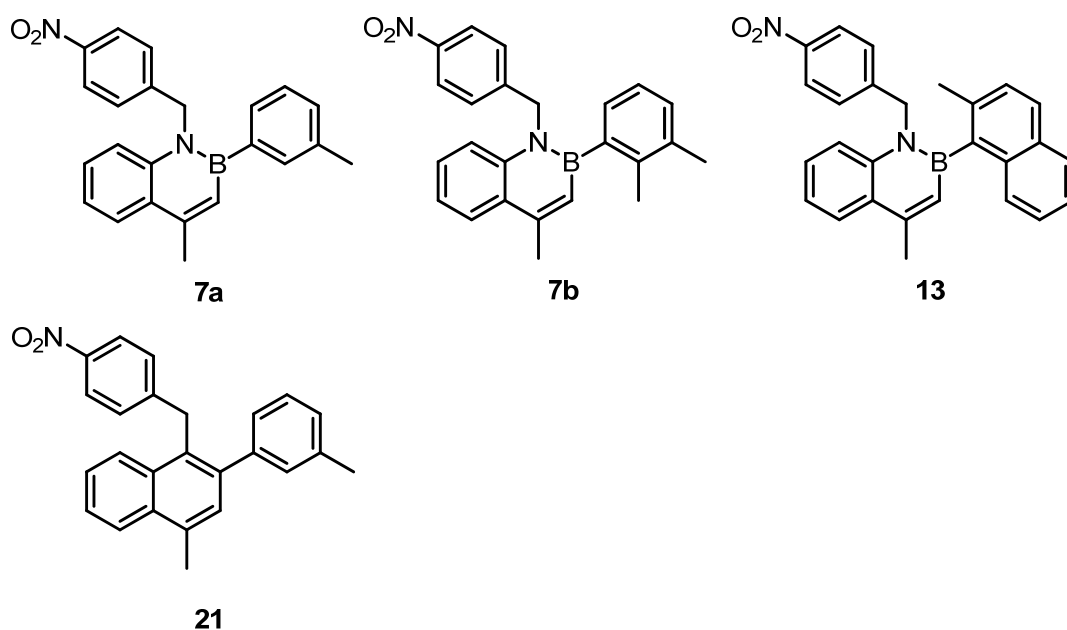
The studied molecules are shown in the scheme below:

Scheme 3. Synthesized and studied compounds

The azaborines possesses a local dipole moment on N-B bond and this can influence the behavior and rotational energy barriers. In order to compare these features, the isosteric compound of **7a** with replacement of N-B by two sp^2 carbon atoms (**21**) was synthesized and analyzed.

The rotational energy barrier was changed by increasing the bulkiness of the aryl groups on boron, from *m*-tolyl to 2-methylnapthyl and CH_2 of the benzylic group on nitrogen was used as a chirality probe to detect the molecular symmetry.

For each molecule, the investigation was carried out according to a standard scheme which can be summarized as shown below:

a) Computational DFT studies are performed to get preliminary information on geometries and the relative energies of the available ground states.

b) DFT optimizations are performed to obtain information about 3D-structure of transition states. The real mechanism of interconversion between two ground states is determined by the transition state with the lowest energy.

c) The rotational energy barriers ($\Delta G^{\#}$) are measured with dynamic NMR and kinetic experiments. The experimental analyses were compared with theoretical predictions.

In the case of compound **7a**, single crystals suitable for X-Ray diffraction analysis were obtained. Theoretical simulation of the Electronic Circular Dichroism spectra (ECD) was used to assign the absolute configuration of stable atropisomers of compound **13**.

3. Results and discussion

1,2-azaborine variously substituted on boron with asymmetric aryl moiety, can generate enantiomeric conformations. In fact the perpendicular disposition of the aryl group with respect to 1,2-azaborine planar framework produces two conformations that are non-superimposable mirror images (Scheme 4).
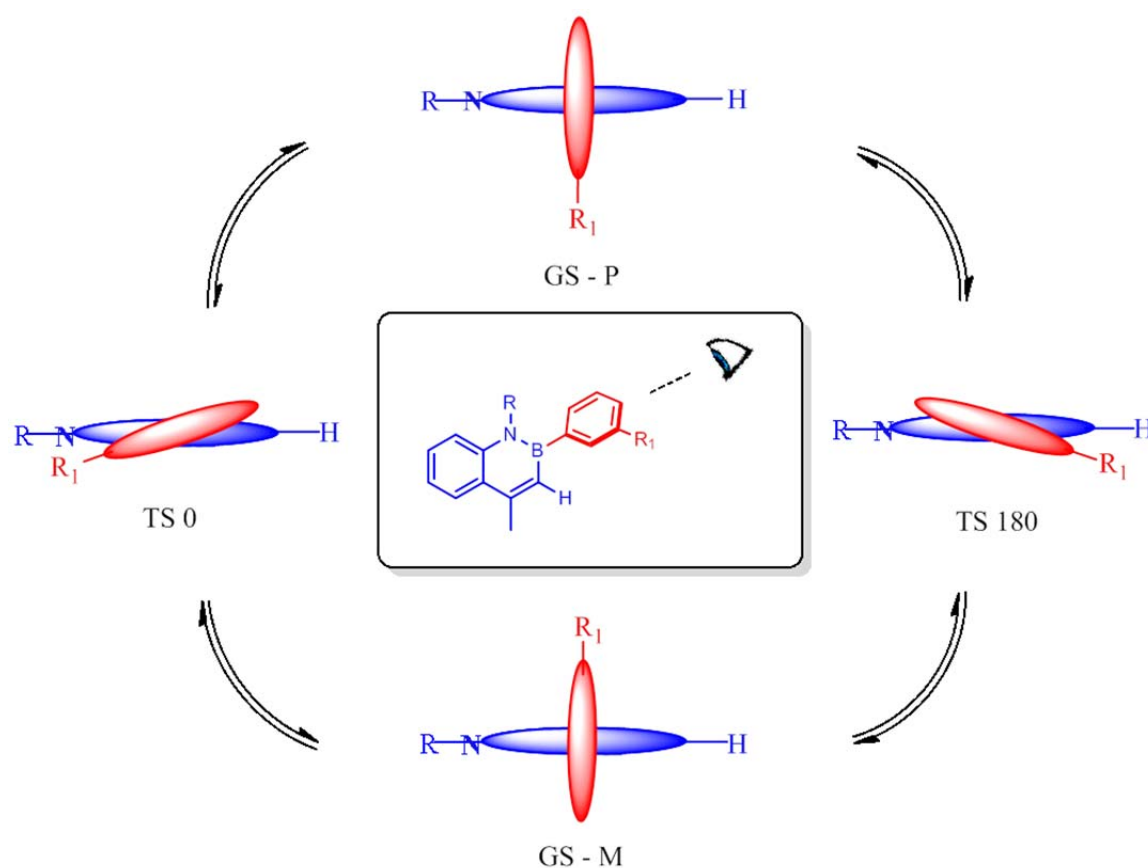
Scheme 4. Schematic rotation of substituted aryl group about the chiral axis.

Depending on the hindrance of the substituents on the aryl ring, the resulting conformations could be stereolabile or configurationally stable.

In order to detect the effects of the B-C stereogenics axis and to determine the energy barrier of this rotation, a chirality probe was installed in position 1 of the 1,2 azaborines derivates. The benzyl group is well suitable to this purpose because the isolated CH_2 display different multiplicity depending on the rotational rate. When the rotation of the group on B-C_{aryl} bond is fast in the NMR timescale a single averaged signal is visible (singlet). When the rotation of the group on B-C_{aryl} bond is slow in the NMR timescale the

CH₂ displays a double doublet (AB system), because the two protons of benzyl group become diastereotopics (Figure 7).
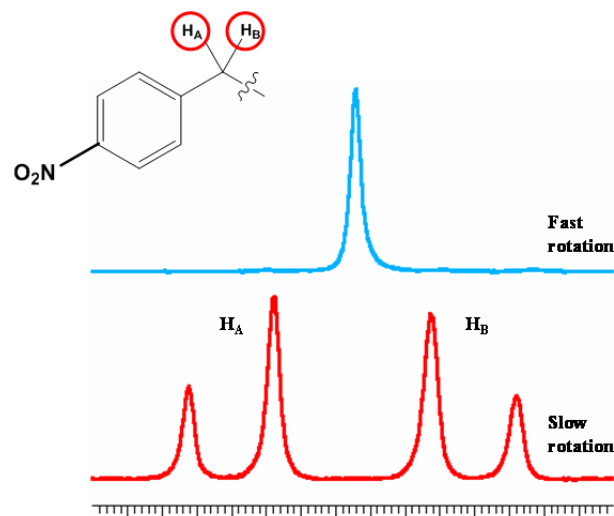
Figure 7. Singlet signal and AB system of CH$_2$ at fast and slow rotation in NMR timescale.

In particular, *p*-nitrobenzyl group has been installed for simplify the aromatic region of the proton spectra of the final products.

3.1 Synthesis and conformational studies of 1,2-azaborines 7a-7b

The first molecule that was synthesized and analysed was **7a**, according to the reported procedure by Molander,[26] the synthesis allow to obtain functionalized 2,1-borazaronapthalenes in one step under mild and transition metal-free conditions. The product was obtained with good yield starting from *N*-substituted 2-aminomethylstyrene and a potassium organotrifluoroborate converted to the active specie Aryl-BCl$_2$ in situ by addition of a fluorophile (Scheme 5).
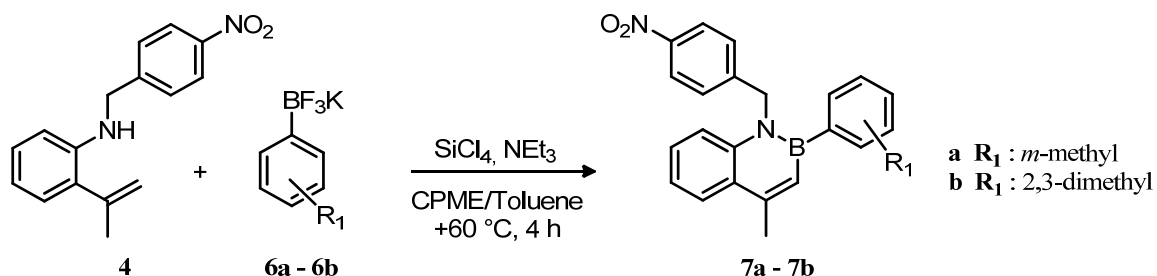
Scheme 5. Synthetic scheme and reaction conditions used to prepare 7a and 7b.

DFT calculation for compound **7a** were run at the B3LYP/6-31G level of theory to explore the conformational space due to all different dispositions of the benzyl and the *m*-tolyl moieties.

Taking into account a single enantiomer due to the stereogenic axis (*P*), four stable conformations were found. They differ because of different relative disposition of 3-methyl substituent and the benzyl moiety that can be on the same side (*syn*) or on the opposite side (*anti*), respectively.

Moreover, for each of these two conformations, two additional conformers are generated by the different dihedral angle of the *m*-tolyl ring (≈+60° and ≈+120°, see Figure 8)

Ground states 7a

anti-(+130°)
$\Delta G^{\#} = 0.00$ kcal/mol

anti-(+61°)
$\Delta G^{\#} = 0.60$ kcal/mol

syn-(+122°)
$\Delta G^{\#} = 0.56$ kcal/mol

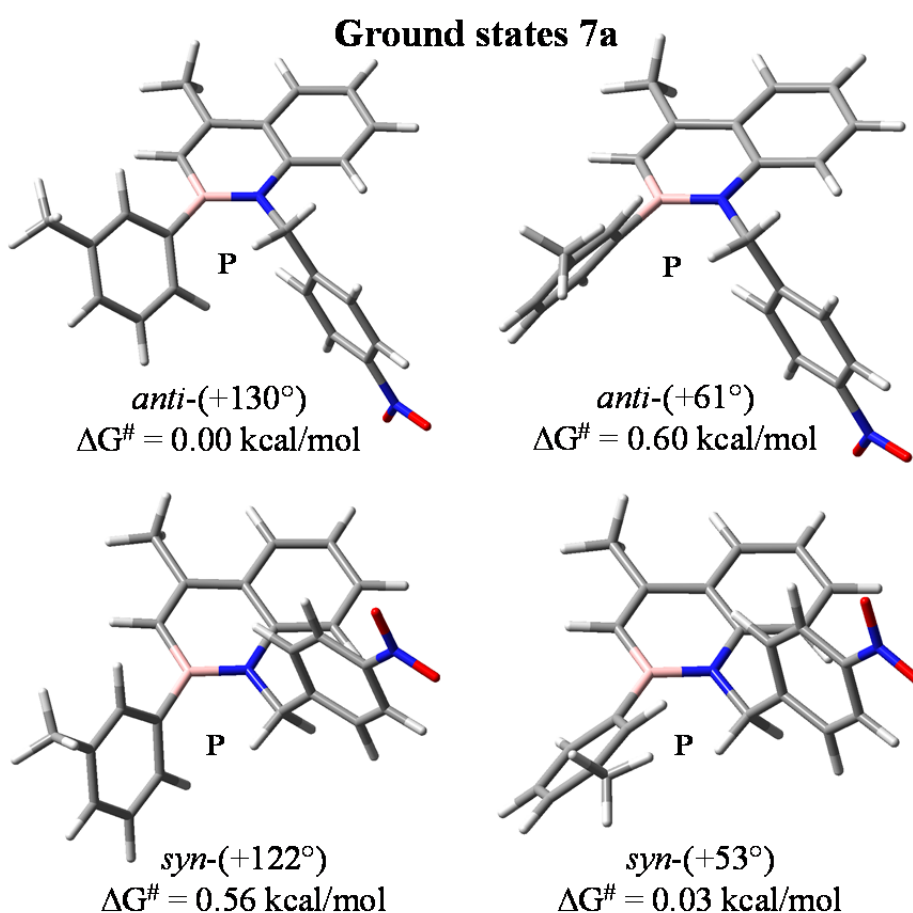*syn*-(+53°)
$\Delta G^{\#} = 0.03$ kcal/mol

Figure 8. Ground states geometries and relative calculated energies of compound 7a.

The four conformation have very similar energies, thus all of them should be populated.

To theoretically analyze the stereodynamic pathways, DFT optimizations of transition states were run and the theoretical results have proved to be coherent in most of the cases.

As shown in Figure 9, four transition states were found: two transition states due to the rotation of aryl moiety and other two because of rotation of benzyl group.

TS for *p*-nitrophenyl rotation 7a

TS1
$\Delta G^{\#} = 10.5$ kcal/mol

TS2
$\Delta G^{\#} = 14.2$ kcal/mol

TS for methylphenyl rotation 7a

TS0
$\Delta G^{\#} = 6.5_3$ kcal/mol

TS180
$\Delta G^{\#} = 6.4_8$ kcal/mol
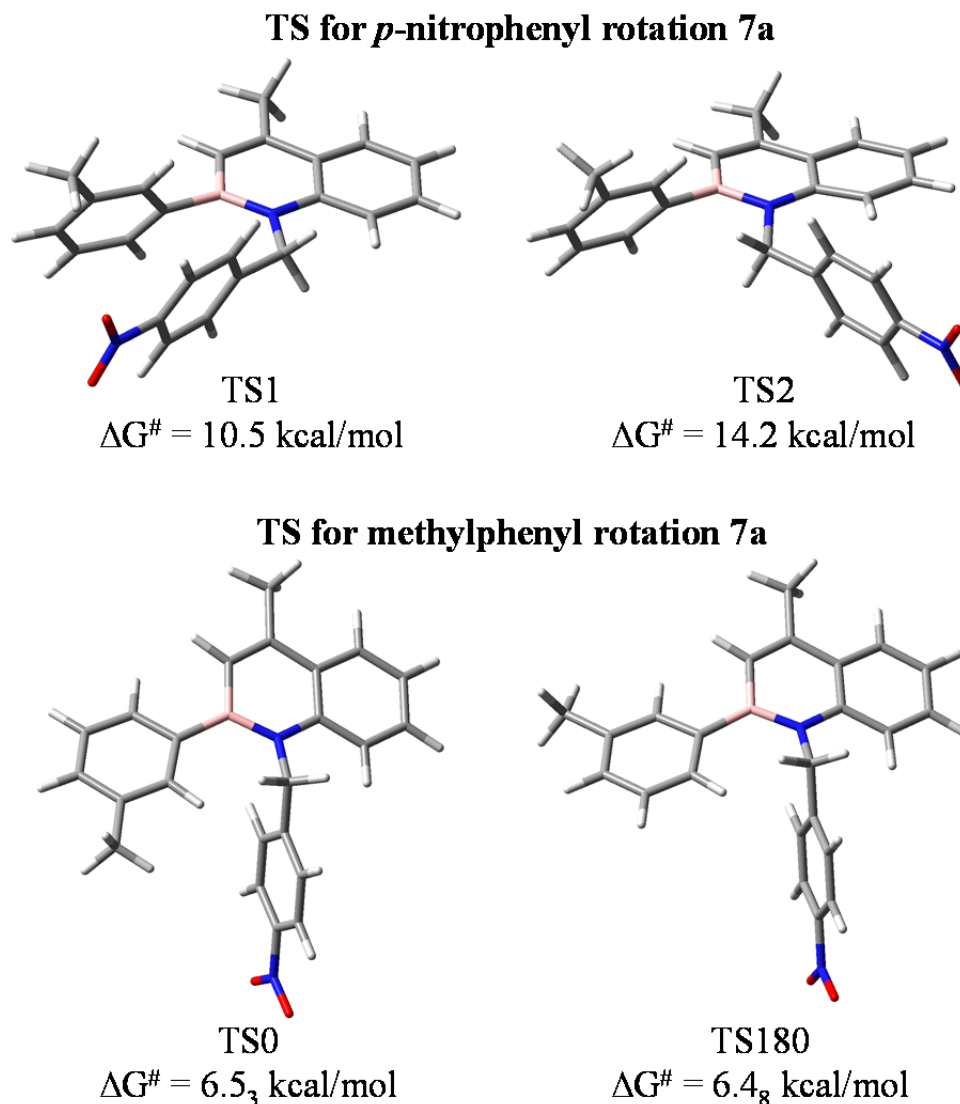
Figure 9. Possible transition states and relative calculated energies.

The favored transition state of interconversion among two ground states is the transition state that has the lowest energy. Therefore, the best stereodynamic pathways for compound **7a** were represented respectively by TS1 and TS180: the first for the rotation of benzyl group and the second for the rotation of aryl group. Surprisingly, the more favorable transition state for benzyl rotation puts the two aryl rings perfectly stacked. Thus, by slowing the rotation of benzyl moiety conformational enantiomers were obtained (higher barrier) whereas conformational diastereomers could be observed by freezing the rotation around B-C$_{aryl}$ bond (lower barrier).

In light of these results, there was the necessity to experimentally evaluate and compared the results with theoretical predictions and for this purpose variable-temperature NMR spectroscopy was used.

On lowering the temperature of a CD_2Cl_2 sample of **7a**, the CH_2 signal started to broad below -12 °C, reached the coalescence at -37 °C and eventually split into two doublets at -89 °C (Figure 10). At this temperature, in the NMR timescale, the highest barrier is frozen and the AB system is observed because of the presence of conformational enantiomers. Line shape simulations provided the rate constants for the rotational process at each temperature, and hence the free energy of the process that is $10.7 \pm 0.1_5$ kcal/mol for azaborine **7a**.

Figure 10. VT spectra for compound 7a (^{1}H-NMR 600 MHz in CD$_2$Cl$_2$). On the left is shown the evolution of the CH$_2$ signal on lowering the temperature. On the right are reported the lineshape simulations with the corresponding rate constants. *Signal of the solvent.

In order to investigate and evaluate the diastereomerization barrier, CDFCl$_2$ was used to reach lower temperatures. On further lowering the temperature a new broadening of the signals due to the slowing of the rotation around B-C$_{aryl}$ bond was observed below -128 °C.
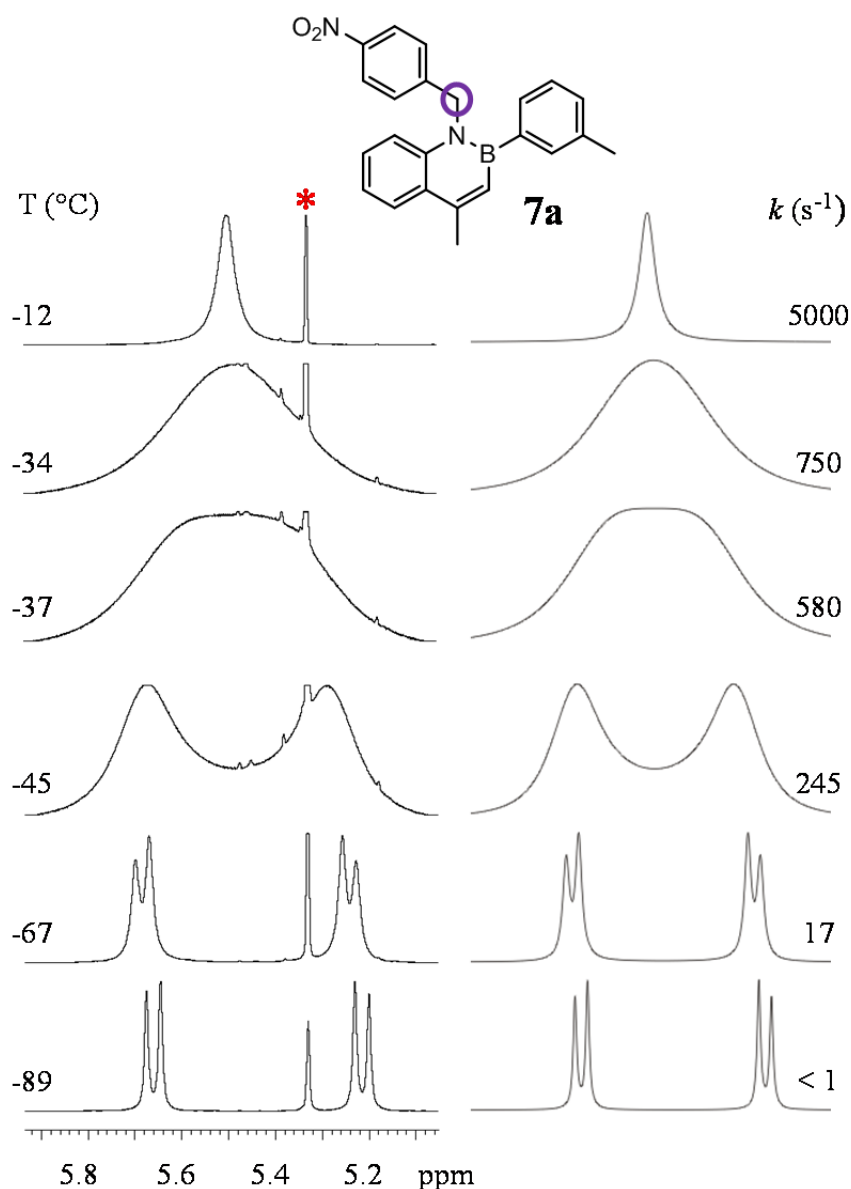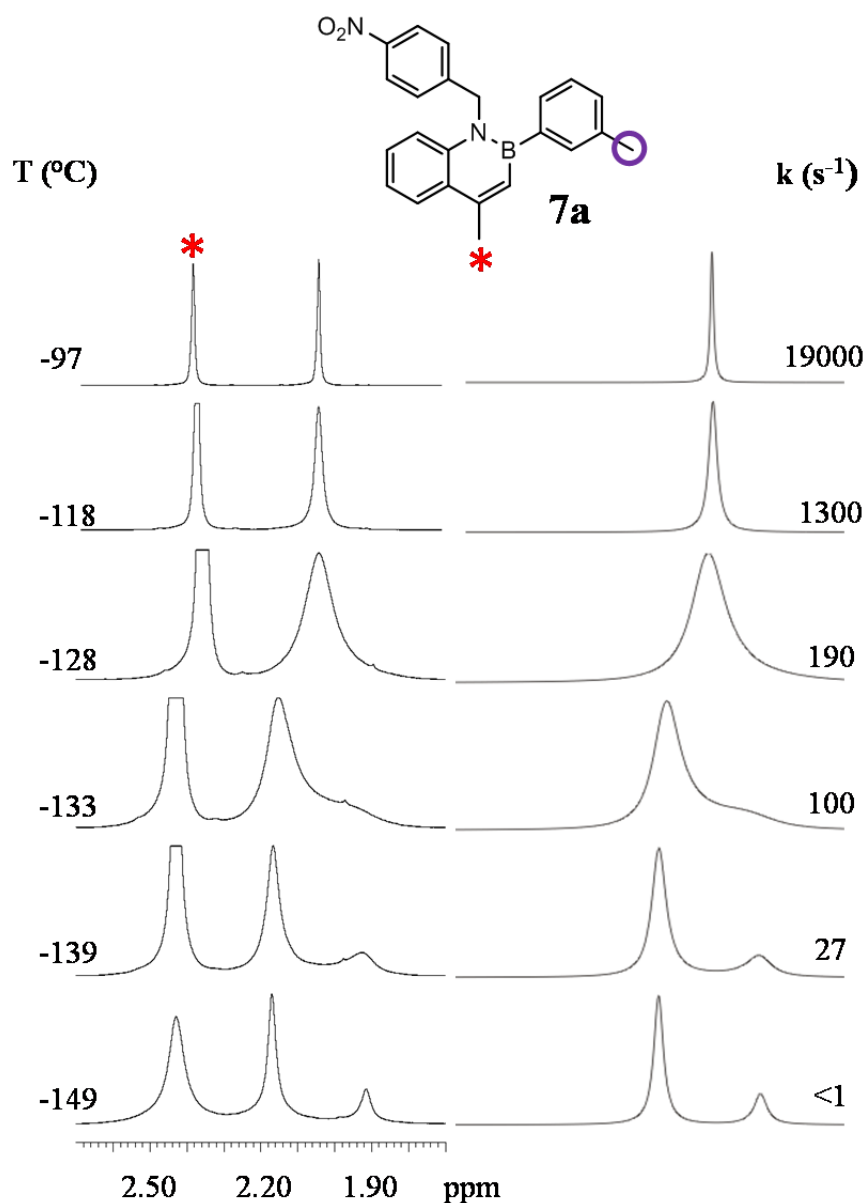
Figure 11. VT spectra for compound 7a (^{1}H-NMR 600 MHz in CDFCl$_2$). On the left is shown the evolution of the *meta* CH$_3$ of B-aryl on lowering the temperature. On the right are reported the lineshape simulations with the corresponding rate constants. *Signal of CH$_3$ of azaborine cycle.

The *meta* CH$_3$ signal broadens below -128 °C, reaches the coalescence at -133 °C and splits in two singlets with relative ratio 77:23 at -149 °C (Figure 11).

The unbalanced ratio confirmed that the two conformational diastereomers were present, thus both the rotational barrier must be frozen.

Line shape simulations obtained for the CH$_3$ signals provided a diastereomerization barrier of 6.7 kcal/mol, in good agreement with the value suggested by DFT for B-Aryl rotation.

Single crystals of **7a** were obtained by slow evaporation of a dichloromethane solution and X-ray diffraction analysis was performed.

Literature data on this kind of compounds are rare. Seki and Hatakeyama reported the crystal structure of a B-N fused polyciclic aromatic structure where the azaborine substructure was twisted by steric interaction, reporting a B-N bond distance of 1.426 Å, typical B=N bond.[27]

Most likely, this is the first crystal structure of a 1,2-azaboranapthalene with N-C and B-C bonds (Figure 12) and a detailed description of the bond lengths can therefore cast new light on the electronic features of these compounds. The compounds crystallizes in the centrosymmetric P2$_1$/n point group, so both the conformational enantiomers are present in the unit cell. Each cell is composed of 4 molecules of **7a**. The arrangement of **7a** determined by X-ray analysis is very similar to the *anti-(+61°)* ground state hinted by DFT calculations.
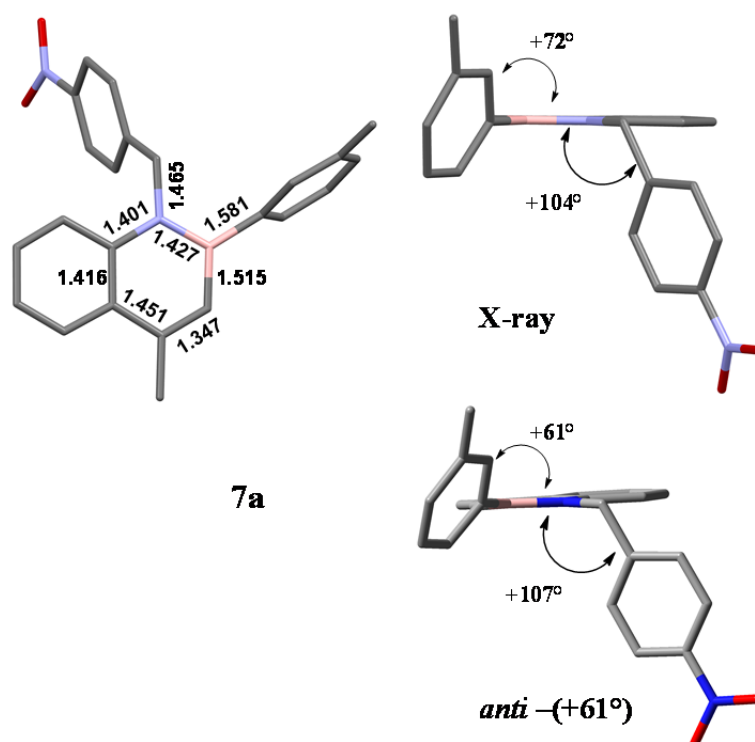
Figure 12. At the top X-ray structure of compound 7a is reported (crystals from CH$_2$Cl$_2$). Top left are reported some relevant bond lengths. Top right: a side view of 7a. At the bottom is reported conformation anti-(+61°) of GS by DFT calculations. Hydrogen atoms are omitted for clarity.

The 1,2-Azaboranapthalene ring is perfectly planar and the B-N bond length is 1.427 Å (in good agreement with the structure reported by Seki and Hatakeyama), shorter than the C$_4$-C$_5$ bond length. The short bond length determined confirms the strong contribution of

16

the nitrogen lone pair to develop a double bond between nitrogen and boron. On the contrary the B-C_3 bond length (1.505 Å) is more consistent with a B-C single bond and C_3-C_4 length is typical of an isolated C=C double bond. The structure in the solid state has the 3-methylphenyl group displaced out of the azaborine plane by 72°, and the *p*-nitrophenyl group is almost perpendicular to the same plane (B-N-CH_2-Cq dihedral angle = 104°). Due to the twisted conformation, the *m*-tolyl ring cannot develop conjugation with boron, and the B-Cq bond length is 1.581 Å.

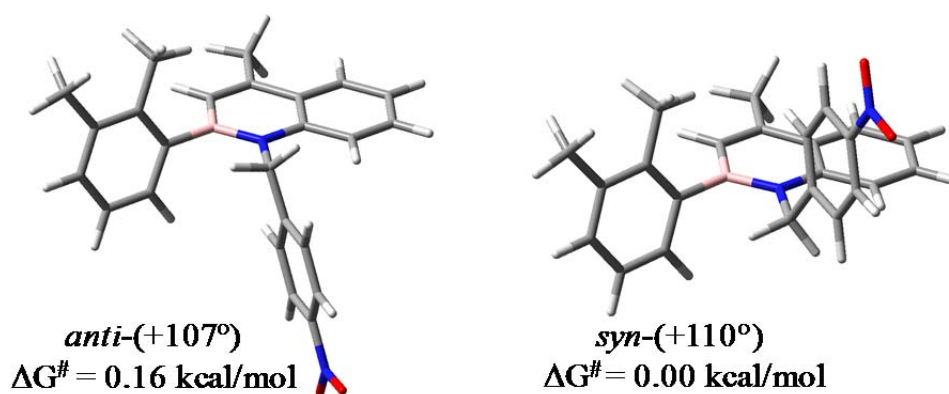Molecule **7b** was synthesized with the same procedure shown in Scheme 5 and good yields were obtained. Hence, DFT calculations were performed in order to compute the ground states and transition states to look for the favorable stereodynamic pathway.

In this case, taking into consideration a single enantiomer (*P*) two different ground states have been found: the two methyl groups and *p*-nitrobenzyl moiety could be on the same side (*syn*) or on the opposite side (*anti*) with respect to the azaborine plane (Figure 13). Regarding the transition states, as in the case of compound **7a**, four geometries have arisen and DFT calculation suggested, this time, enantiomers are obtained by freezing the rotation around B-C_{aryl} (higher barrier) and diastereoisomers could be obtained by blocking the rotation of *p*-nitrobenzyl moiety (lower barrier).

Ground states 7b

anti-(+107°)
ΔG$^{\#}$ = 0.16 kcal/mol

syn-(+110°)
ΔG$^{\#}$ = 0.00 kcal/mol

TS for 2,3-dimetylphenyl rotation 7b

TS180
ΔG$^{\#}$ = 16.5 kcal/mol

TS0
ΔG$^{\#}$ = 23.1 kcal/mol

TS for *p*-nitrophenyl rotation 7b

TS1
ΔG$^{\#}$ = 10.0 kcal/mol

TS2
ΔG$^{\#}$ = 13.4 kcal/mol
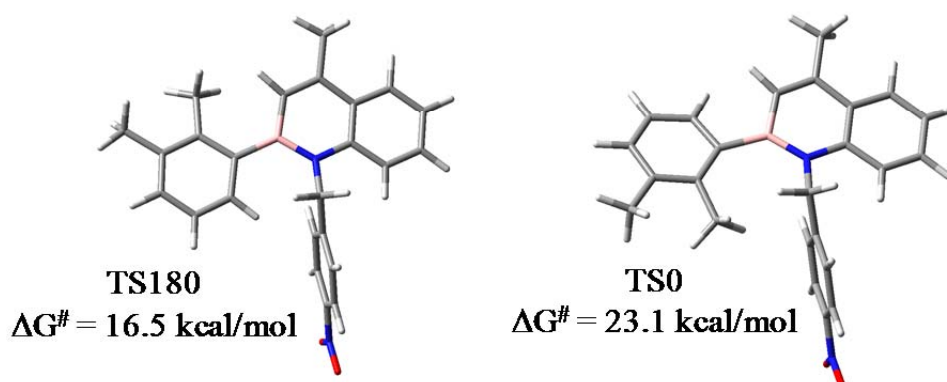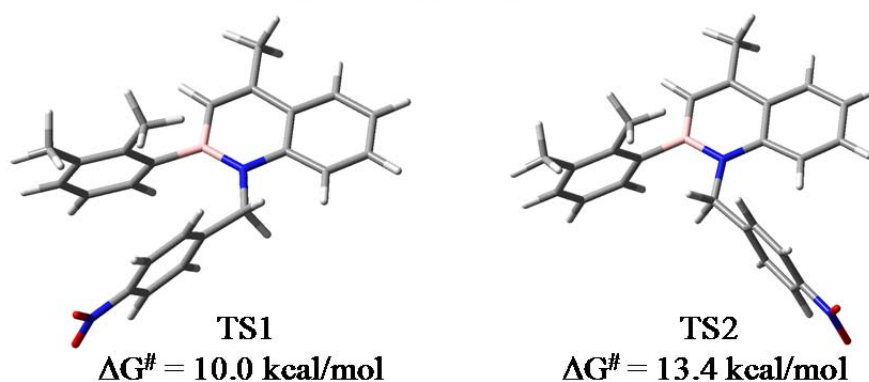
Figure 13. Ground states and transition states geometries of compound 7b and relative energies.

This theoretical predictions were experimentally evaluated by dynamic NMR.

At room temperature the spectrum of compound **7b** exhibits a well resolved AB system for the benzylic group CH$_2$, albeit with much smaller chemical shift separation with respect to compound **7a** (36 Hz for **7b** and 267 Hz for **7a**, respectively). Therefore, two

enantiomeric conformations are already present and it is necessary to increase the temperature to evaluate the higher barrier. On raising the temperature, a broadening of AB system is shown at +82 °C and the coalescence point is reached at +111 °C and a single peak is observed above +130 °C (Figure 14). The corresponding energy barrier derived from lineshape simulations is 19.1 kcal/mol. This barrier can be safely assigned to the B-aryl rotation due to the relevant steric hindrance due to the *ortho*-methyl, and the calculated value is in fair agreement with the experimental value (see Table 1 at the end of the chapter 3).
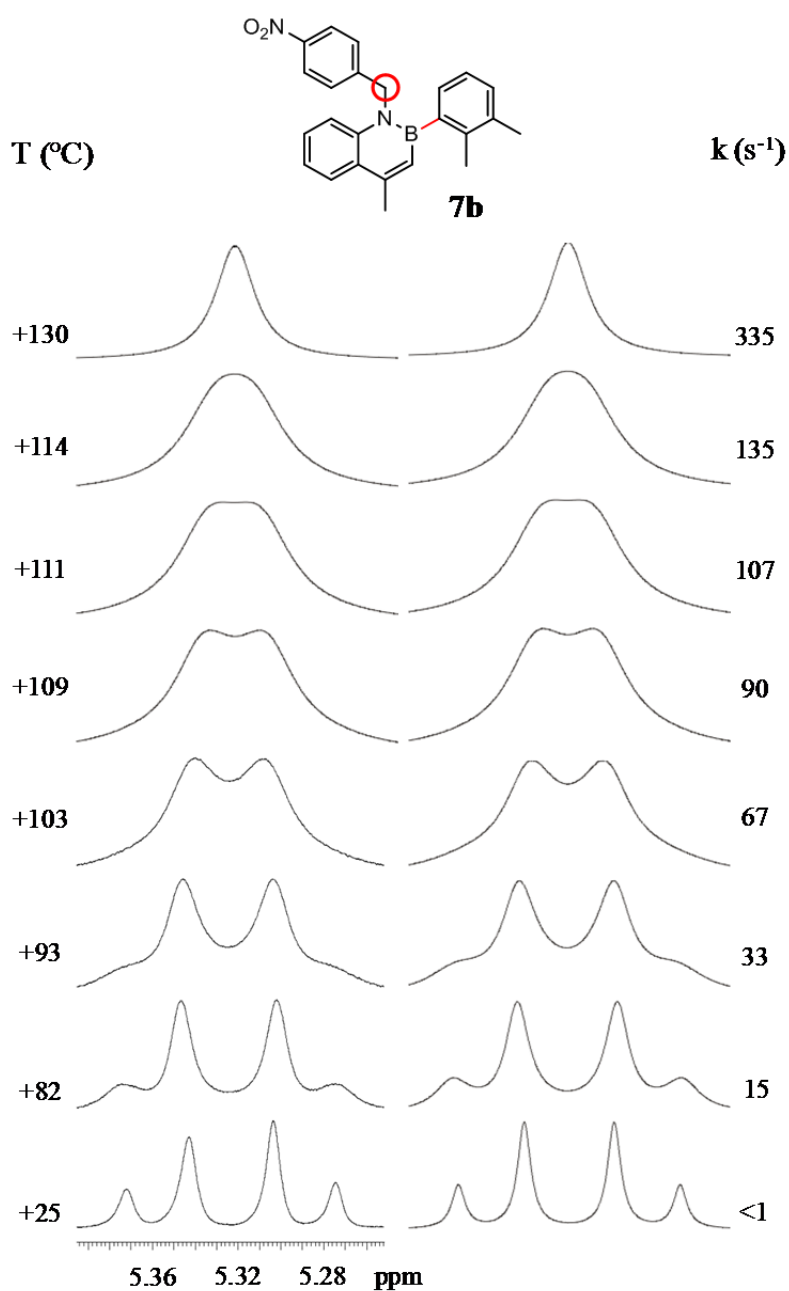
Figure 14. VT spectra for compound 7b (^{1}H-NMR 600 MHz in $C_2D_2Cl_4$). On the left is shown the evolution of the CH$_2$ signal on raising the temperature. On the right are reported the line shape simulations with the corresponding rate constants.

When a sample of **7b** in CD_2Cl_2 was cooled down, the two doublet of AB system broaden and split at -90 °C in two pairs of signals with 75:25 ratio, thus confirming the formation of two conformational diastereoisomers by the two stereogenic axes (Figure 15). The experimental energy barrier determined by lineshape simulation was 10.0 kcal/mol, very similar to the higher barrier of compound **7a** and identical to that suggested by calculations for N-benzyl rotation.

This unambiguously confirms that the enantiomerization barrier investigated for **7a** was due to the freezing of the rotation around $N-CH_2$ bond.
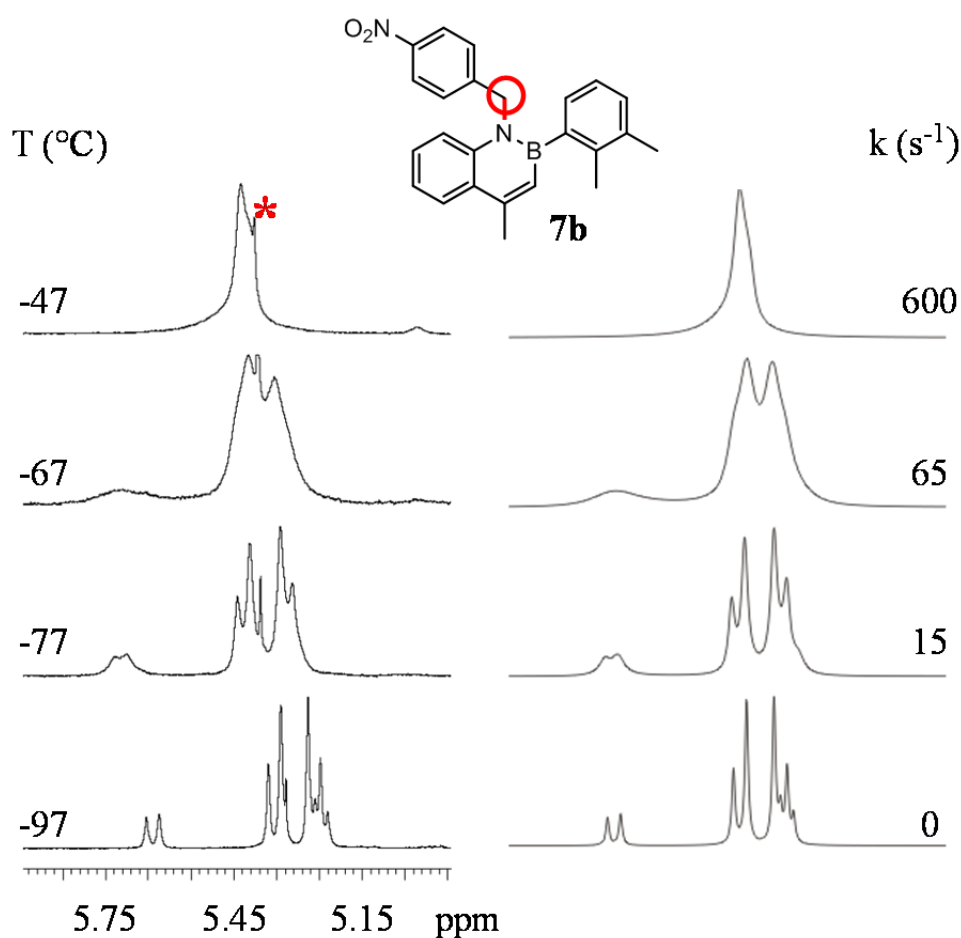
Figure 15. VT spectra for compound 7b (^{1}H-NMR 600 MHz in CD$_2$Cl$_2$). On the left is shown the evolution of the CH$_2$ signal on lowering the temperature. On the right are reported the lineshape simulations with the corresponding rate constants. * Signal of the solvent.

3.2 Synthesis and conformational studies of compound 13

Albeit rather high, the B-aryl rotational barrier for compound **7b** does not allow for a physical resolution of the atropisomeric pair. For this purpose we prepared compound **13**, bearing the 2-methylnapthalene moiety. DFT calculations suggested an enantiomerization barrier of about 31 kcal/mol for this compound.

Due to the steric hindrance, compound **13** cannot be prepared with the simpler procedure employed to synthesize **7a** e **7b,** but it had to be prepared by the procedure suggested by Dewar.[28] Once synthesized **10**, by the addition of 2-methylnaphthylmagnesium bromide to the 2-chloro-2,1-borazaronapthalene (**Int**) preformed in situ, then lithiation with *n*-BuLi/TMEDA and alkylation provided compound **13** (Scheme 6).
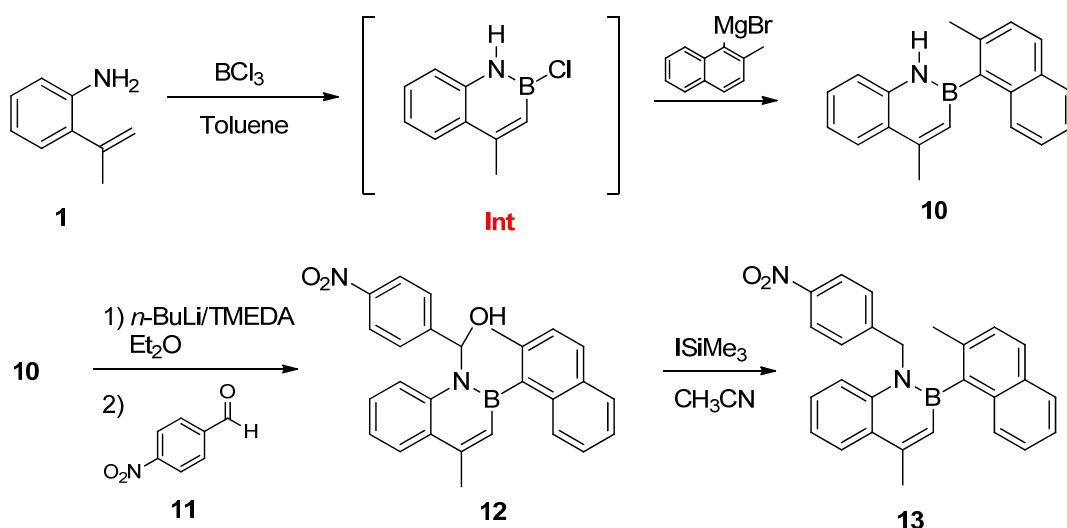
Scheme 6. Synthetic scheme used to prepare 13.

Taking into account a single enantiomer (*P*-**13**), DFT calculations hinted that only two ground states are populated (Figure 16). This result is due to the steric hindrance of 2-methylnapthyl moiety. The more steric hindrance it is, the more the bulky group prefer to be perpendicular to the azaborine plane.

Ground states 13

anti-(+81°)
$\Delta G^{\#}$ = 0.00 kcal/mol

syn-(+104°)
$\Delta G^{\#}$ = 0.31 kcal/mol
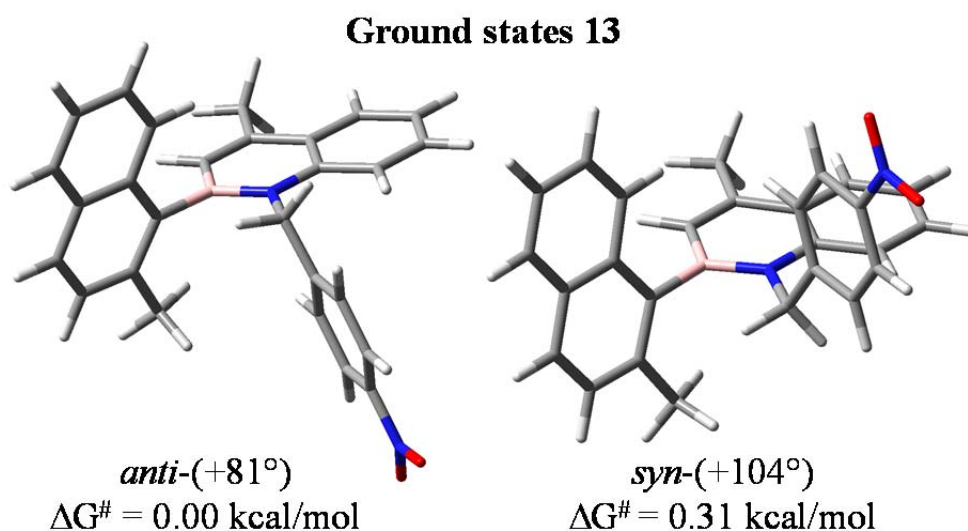
Figure 16. Ground states geometries and relative calculated energies of compound P-13.

The lowest energy of conformations for compound **13** is represented by *anti* dispositions, where the second ring of naphthalene is on the opposite side to the phenyl of the *p*-nitrobenzyl moiety. Regarding the transition states, TS180 seems to represent the most favourable stereodynamic pathway for the interconversion of the two conformational enantiomers (Figure 17).

TS for methylnaphthyl rotation 13

TS0
$\Delta G^{\#}$ = 31.3 kcal/mol

TS180
$\Delta G^{\#}$ = 31.0 kcal/mol
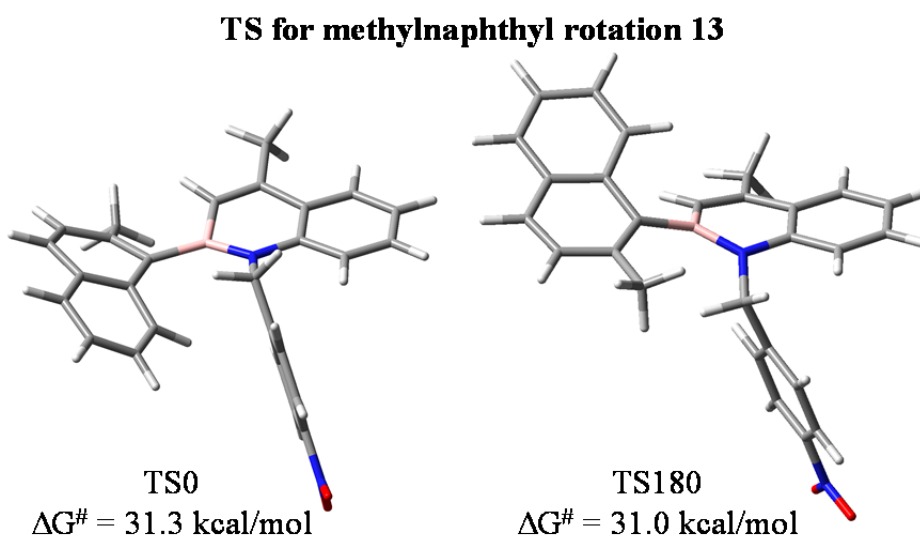
Figure 17. Possible transition states geometries and relative calculated energies of compound 13.

At room temperature ^{1}H-NMR spectrum shows a slightly broadened AB system.

On raising the temperature up to +130 °C the broadening of the double doublet wasn't observed and therefore this time dynamic NMR approach didn't allow to experimentally

evaluate the free energy barrier of the interconversion process. Being higher than 22-23 kcal/mol, the racemization barrier was determined by kinetic analysis.

The atropisomeric pair was resolved by means of enantioselective HPLC on Chiralpak AS-H column, with good separation between the two atropisomers (Figure 18).
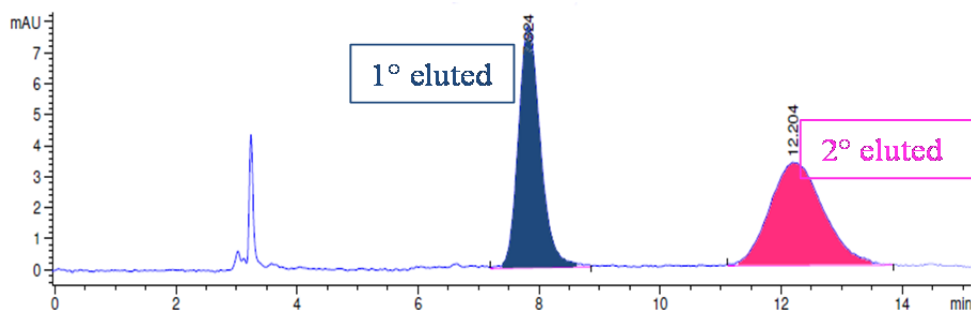
Figure 18. HPLC chromatogram (AS-H column, hexane : *i*-Pr = 9 : 1, 1 mL/min).

The racemization process was followed by means chiral HPLC with the same elution conditions, keeping the enantiopure sample at a constant temperature (+130 °C) and by recording the HPLC data at different times in order to evaluate the changing enantiomeric ratio.

For this purpose, a small amount of pure enantiomer was dissolved in 1 mL of $C_2D_2Cl_4$ and was kept into an hot and stirred oil bath. The temperature of the oil bath was controlled by using a thermocouple. Although $C_2D_2Cl_4$ has an high boiling point (+146.5 °C), its good vapor pressure allows to easily evaporate it before injection in HPLC column.

Once racemization was reached, the experimental values were collected and interpolated by a first order reversible kinetic equation and the rate constant (*k*) values referred to each experimental temperature were obtained (Equation 1).

$$M \underset{}{\overset{k}{\rightleftharpoons}} P$$

$$\ln(x - x_{eq}) = \ln(x_0 - x_{eq}) - 2k \cdot t$$
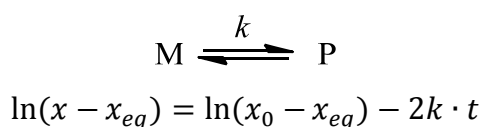
Equation 1. First order reversible kinetic and corresponding equation.

Where *x* is the molar fraction of the enantiomer that is interconverting; x_{eq} is the molar fraction of the same enantiomer reached at the equilibrium state (0.5); x_0 is the initial molar fraction of the chosen enantiomer at t_0; *k* is the rate constant (s^{-1}); *t* is the time steps

(s). This equation represent a straight line in the form *y = mx + q*, where the slope is *(-2k)*; the y-intercept is *ln (x₀-xₑq)* and *t* is the variable of the function.

The racemization process was followed at +130 °C and a *k* of $1.287*10^{-5}$ was obtained. Once calculated the k values (s^{-1}), free activation energy at each temperature was determined by means Eyring equation (Equation 2).

$$\Delta G^{\neq} = 4.574 * 10^{-3} * T * (log \frac{T}{k} + 10.318)$$

Equation 2. Eyring equation
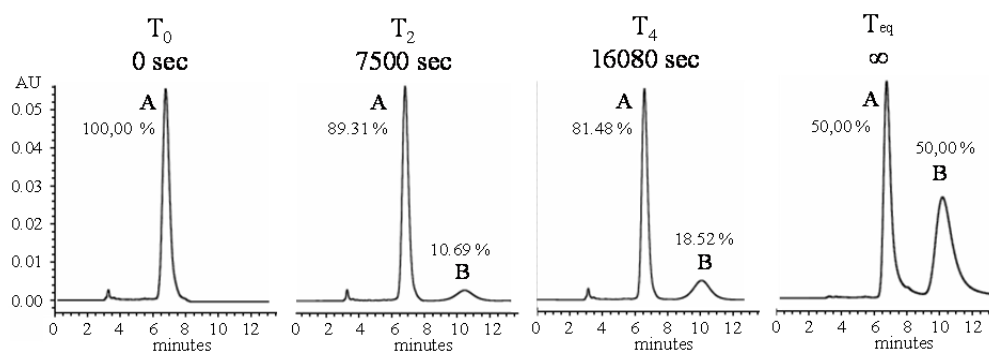
Figure 19. Chromatograms that show the racemization process keeping sample at +130 °C.

	t (s)	ln (xₐ - xₐₑq)
T₀	0	-0,693
T₁	3600	-0,792
T₂	7500	-0,934
T₃	11640	-1,020
T₄	16080	-1,156
T₅	26880	-1,381

slope	-2,57E-05
2k₁	2,57E-05
k₁	1,287E-05
T (°C)	+130
$\Delta G^{\neq}$ (kcal/mol)	**32,8**

y = -3E-05 x - 0,714
R² = 0,991

Figure 20. Kinetic data of first eluted atropisomer fitted with linear regression.

24

Therefore, a free energy of rotational process of 32.8 kcal/mol was determined.

This value is in good agreement with the lowest one resulting from theoretical predictions. Hereafter we will get further data by means other kinetic analysis at different temperatures in order to average the ΔGs determined.

Taking into account the errors in the determination of the sample temperature (±1 °C), the free energies can be considered invariant with the temperature, thus implying a negligible activation entropy.

3.2.1 Assignment of absolute configuration to atropisomers of compound 13

Having in hand the two separated atropisomers absolute configuration were assigned.

In the last years the determination of the absolute configuration of chiral molecules using chirooptical techniques like optical rotation (OR), electronic circular dichroism (ECD), and vibrational circular dichroism (VCD) gained feasibility and reliability because of the development of theoretical methods for the prediction of these properties based on DFT and on the time-dependent density functional theory approach (TD-DFT).ref

In this case, the absolute configuration of the atropisomers of compound **13** were assigned by ECD method.
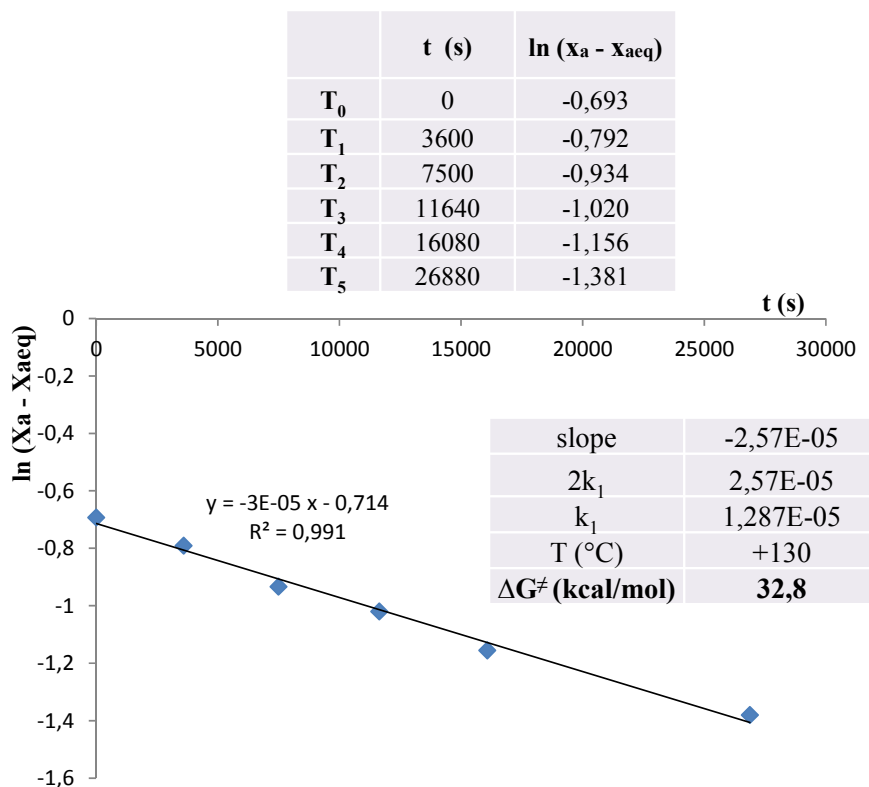
The ECD spectrum of **13** was acquired in HPLC-grade acetonitrile solution ($\approx 6 \cdot 10^{-5}$ M) with a cell path of 0.5 cm in the 190-400 nm region by the sum of 8 scans at 50 nm/min scan rate, using a JASCO J-810 spectropolarimeter (Figure 21).
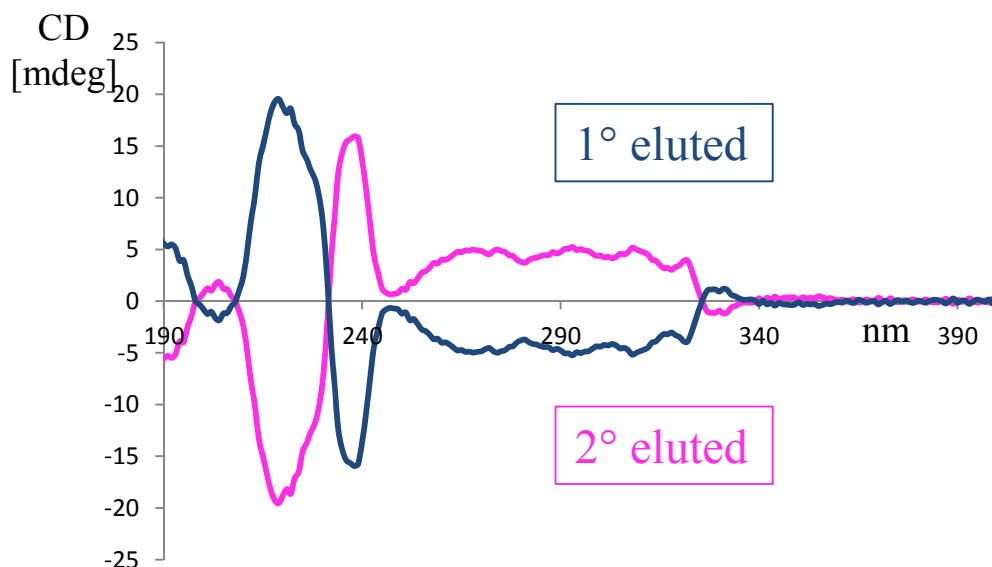
Figure 21. Experimentally ECD spectra of first eluted (blue) and second eluted (pink).

Taking into account the second eluted atropisomer (pink trace), the experimental ECD spectrum exhibits four Cotton effects at 331, 238, 220 and 206 nm and a broad and complex positive branch at 250-310 nm.

The conformational search performed on **13** showed that this compound has two populated conformations (*anti* and *syn*) that have different energies (see Figure 16).

In order to determine the experimental populations, acquisition of ^{1}H-NMR spectrum in CD_2Cl_2 at -100 °C was done, then Boltzmann distribution allow to get the populations of conformers at room temperature that is of 50 % (see Equation 3).

$$\frac{N_{a2}}{N_{b2}} = \left(\frac{N_{a1}}{N_{b1}}\right)^{\frac{T_1}{T_2}}$$

Equation 3. Boltzmann distribution

The ECD spectra of the two conformations were then calculated with cam-b3lyp/6-311++g(2d,p) which is a good functional used for small organic molecules.[29]

The weighted sum of the two calculated spectra of two diastereomeric conformations (*anti* and *syn*) of *P* atropisomer gives the final ECD calculated spectrum of enantiomer *P* (Figure 22).

26
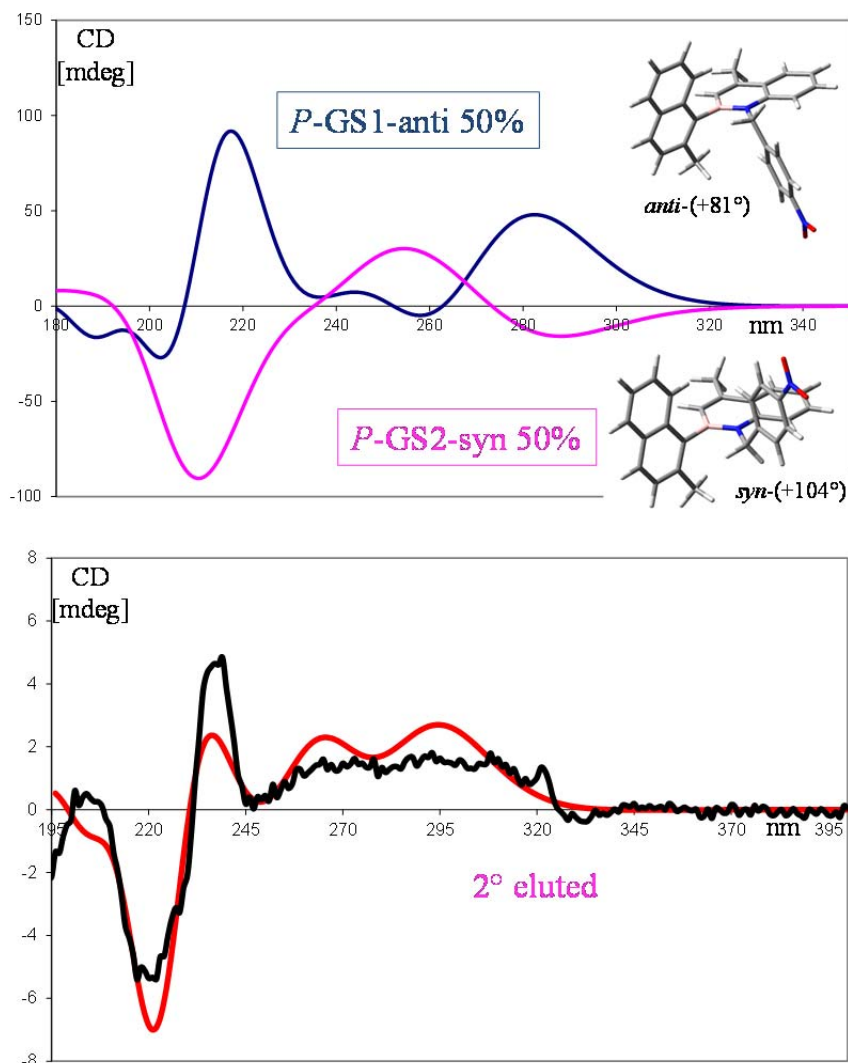
Figure 22. Top: calculated spectra of two conformations of 13. Bottom: weighted sum calculated spectrum (red trace) and experimental spectrum of 2° eluted atropisomer (black trace).

The experimental ECD spectrum of the second eluted enantiomer is in good agreement with the ECD spectrum calculated for *P* atropisomer. For this reason, at the second eluted atropisomer was assigned *P* absolute configuration.

3.3 Synthesis and conformational studies of compound 21

In order to compare the azaborine N-C$_{benzyl}$ and B-C$_{aryl}$ experimental barriers with a isosteric C-C$_{benzyl}$ and C-C$_{aryl}$ compound, **21** was synthesized and used as reference standard. The synthesis involves a Betti reaction of β-napthol with *p*-nitrobenzaldehyde. Removal of piperidine, oxidation, formation of triflate and Suzuki reaction lead to formation of the isosteric product of **7a** where N-B bond is preplaced by C=C bond (*see experimental section*).

27

Taking into account a single enantiomer (*P*), as in compound **7a**, DFT calculations found again four ground states due to the combination between two different dihedral angles for the aryl substituent and two different position of *p*-nitrophenyl moiety (Figure 23).

Ground states 21

anti-(+124°)
$\Delta G^{\#} = 0.00$ kcal/mol

anti-(+66°)
$\Delta G^{\#} = 0.47$ kcal/mol

syn-(+117°)
$\Delta G^{\#} = 0.43$ kcal/mol

syn-(+59°)
$\Delta G^{\#} = 0.01$ kcal/mol
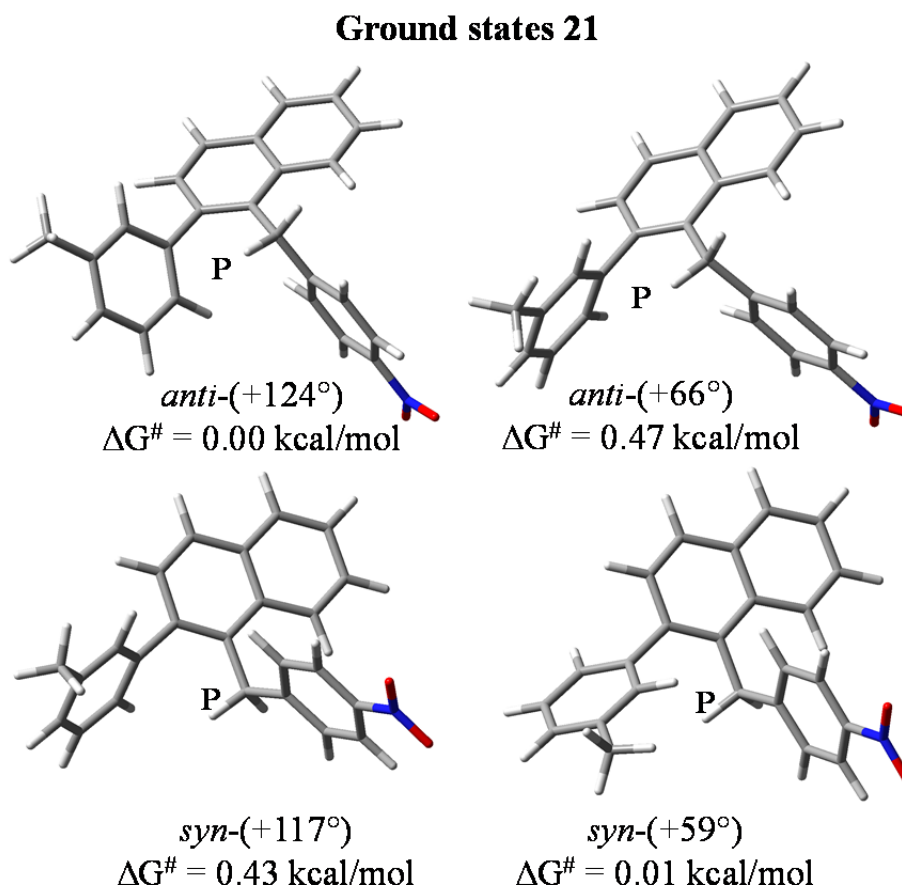
Figure 23. Ground states geometries and relative calculated energies of compound 21.

Regarding the transition states, four geometries have been optimized: two conformations due to the different 3D-dispositon of aryl moiety (TS0 and TS180) and two conformations due to 3D-disposition of *p*-nitrophenyl moiety (TS1 and TS2). As arises from theoretical predictions, this time, the higher barrier is represented by the rotation of asymmetric aryl moiety instead the lower one regards the rotation of benzyl group. This behavior has opposite trend with respect to azaborine **7a** (Figure 24).

The most favorable stereodynamic pathway for the interconversion *anti* to *syn* or *viceversa*, as in compound **7a**, is represented by the situation in which the two aryl groups are perfectly stacked. In this framework the two interconversion pathway are represented by TS0 and TS1. To confirm predicted calculations dynamic NMR was done.

TS for *p*-nitrophenyl rotation 21

TS1
$\Delta G^{\#} = 7.9$ kcal/mol

TS2
$\Delta G^{\#} = 8.3$ kcal/mol

TS for methylphenyl rotation 21

TS0
$\Delta G^{\#} = 11.1_2$ kcal/mol

TS180
$\Delta G^{\#} = 11.1_3$ kcal/mol
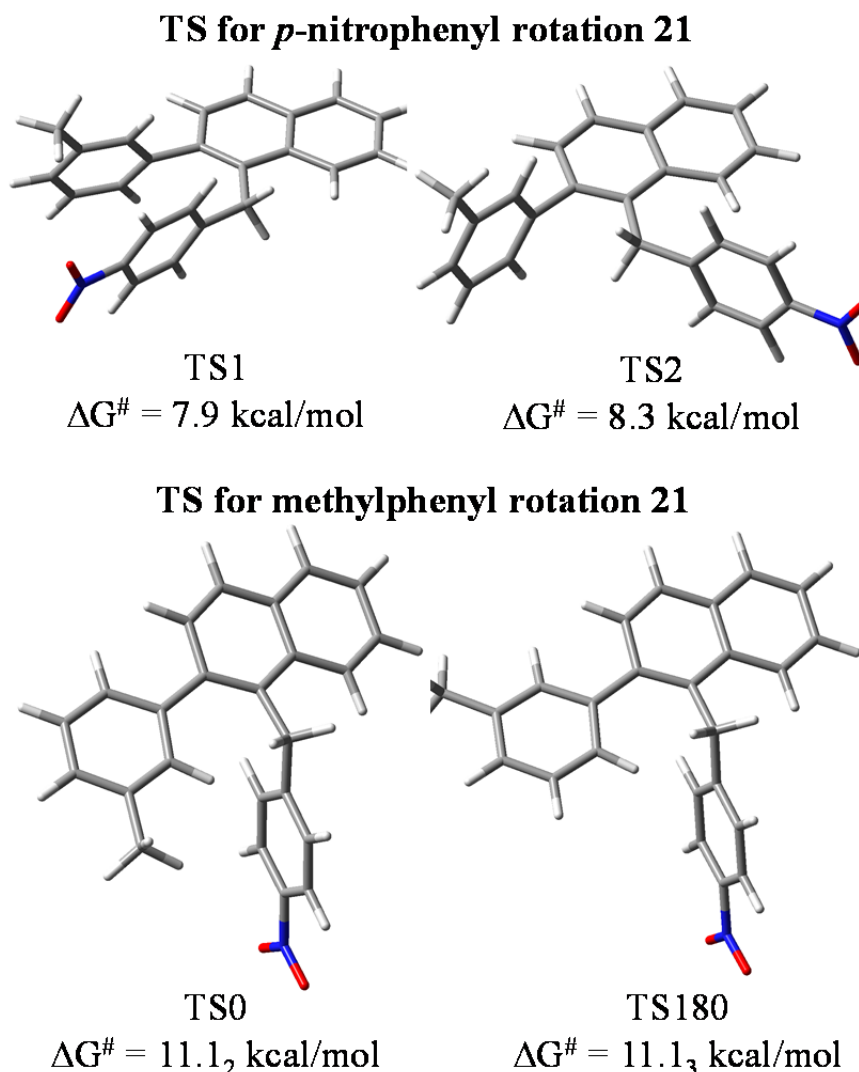
Figure 24. Possible transition states geometries and relative calculated energies of compound 21.

When a sample of **21** in CD_2Cl_2 was cooled, the CH_2 signal of benzyl group starts to broad below -67 °C, reaches the coalescence at -70 °C and eventually splits into a AB system at -83 °C (Figure 25). At this temperature, in the NMR timescale, the enantiomerization barrier is frozen and a strongly coupled AB system is observed due to the existence of conformational enantiomers. Lineshape simulations provide the rate constants for the rotational process, and hence the free energy of the process by using Eyring equation (10.7 kcal/mol).

This experimentally result is in agreement with the values determined for the enantiomerization barrier by DFT calculations (11.1 kcal/mol for *m*-tolyl rotation, see Table 1).

Figure 25. VT spectra for compound 21 (^{1}H -NMR 600 MHz in CD$_2$Cl$_2$). On the left is reported the evolution of CH$_2$ signal on lowering the temperature. On the right are reported the lineshape simulations with the corresponding rate constants.

On lowering the temperature of a CDFCl$_2$ sample of **21** the meta CH$_3$ signal broaden below -87 °C, reaches the coalescence at -104 °C and splits in two singlets with relative ratio 65:35 at -128 °C (Figure 26).

The unbalanced ratio confirmed that the two conformational diastereomers were present, thus both the rotational barriers must be frozen.

Lineshape simulations obtained for the CH$_3$ signals provided a diastereomerization barrier of 8.0 kcal/mol, again in good agreement with theoretical predictions (7.9 kcal/mol for *p*-nitrophenyl rotation).
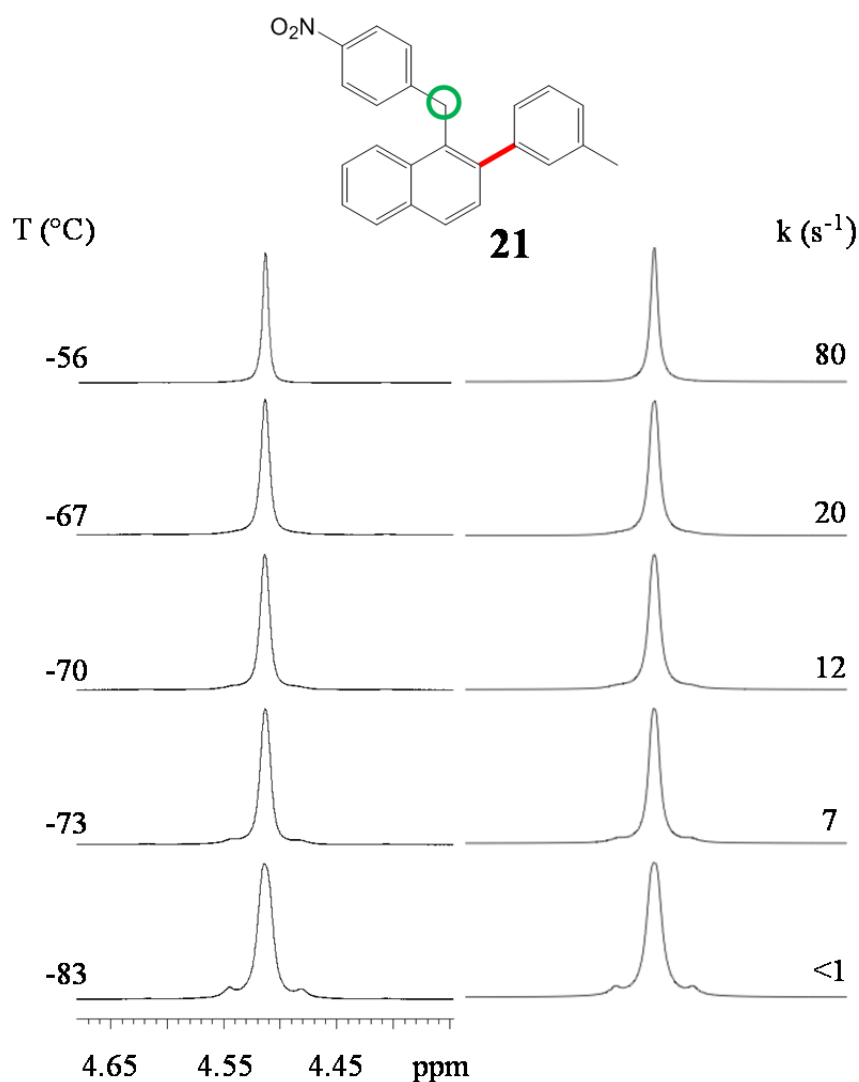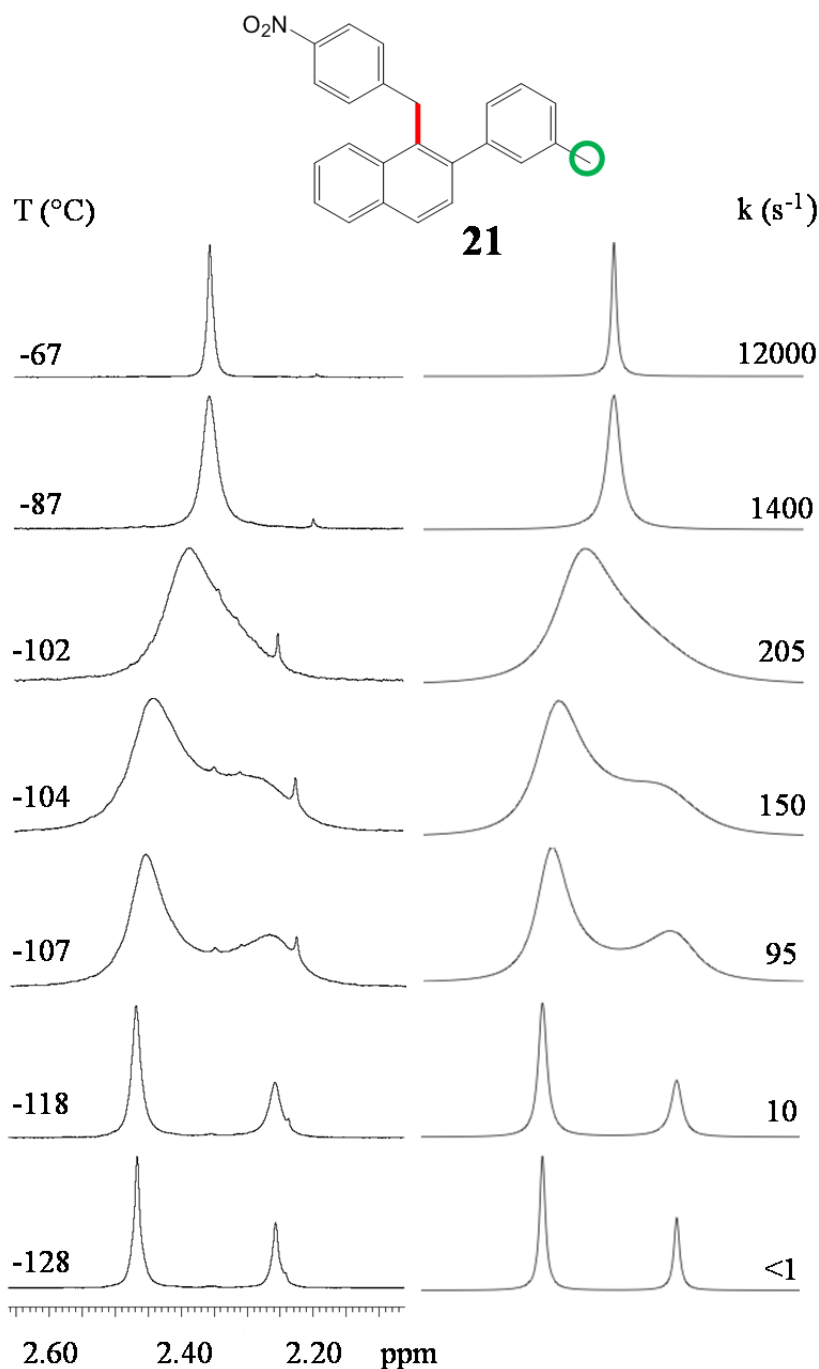
Figure 26. VT spectra for compound 21 (^{1}H -NMR 600 MHz in CD$_2$Cl$_2$). On the left is reported the evolution of CH$_3$ signal of aryl group on lowering the temperature. On the right are reported the lineshape simulations with the corresponding rate constants.

From the comparison between experimentally values and calculated energies of compound **21** seems to arise that $\Delta G^{\#}$ of rotational process of *m*-tolyl group is higher than the $\Delta G^{\#}$ corresponding to the rotational barrier of *p*-nitrobenzyl group. If this supposition were true it would find explanation on the hypothesis in which C$_{naphth}$-C$_{aryl}$ bond (**21**) is shorter than B-C$_{aryl}$ (**7a**) and consequently the aryl substituent is forced to be closer and the rotational barrier raises. On the other hand, a second scenario could

rationalize the lowering of the rotational barrier to a different conjugative contribution in the transition state, that lowers the energy barrier.

Anyway, future conformational studies on compound **22** (Figure 27) should allow to assign by comparison the relative energy barriers to the respective axes, and to get further data to understand the source of the different energy barrier.
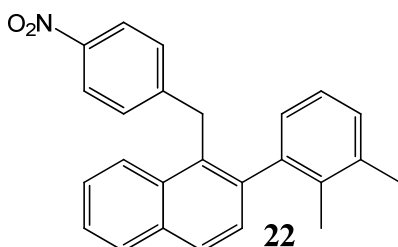
Figure 27. Compound 22 for comparison.

In Table 1 are reported the energy values for both ground and transition states, regarding the *P* enantiomer, derived from DFT calculations for each compound and the relative experimental rotational barriers.

Table 1. Optimized ground and transition states normalized energies of the *P* atropisomer, expressed in kcal/mol, calculated at B3LYP/6-31G(d) level; the *M* enantiomer has the same energy values.

Compound	syn (D)[a] $\Delta G^{\#}$	anti (D)[a] $\Delta G^{\#}$	Rotation of aryl $\Delta G^{\#}$			Rotation of benzyl $\Delta G^{\#}$		
			TS0	TS180	Exper.	TS1	TS2	Exper.
7a (*m*-tolyl)	(+53°) 0.03 (+122°) 0.56	(+61°) 0.60 (+130°) 0.00	6.5_3	6.4_8	**6.7**	10.5	14.2	**10.7**
7b (2,3-dimethyl)	(+110°) 0.00	(+107°) 0.16	23.1	16.5	**19.1**	10.0	13.4	**10.0**
13 (*o*-methylnaphtyl)	(+104°) 0.31	(+81°) 0.00	31.3	31.0	**32.8**	ns	ns	ns
21 (*m*-tolyl)	(+59°) 0.01 (+117°) 0.43	(+66°) 0.47 (+124°) 0.00	11.1_2	11.1_3	**10.7**	7.9	8.3	**8.0**

D[a] dihedral angle   ns = not yet studied

4. Conclusion

In this project thesis we studied the stereodynamic behavior of 1,2-azaborines variously substituted on boron (**7a**, **7b**, **13**). Depending on the hindrance of the asymmetric aryl substituent the resulting conformations could be stereolabile or configurationally stable. Rotational barriers of *m*-tolyl (**7a**) and 2,3-dimethylphenyl (**7b**) were investigated by using variable-temperature NMR approach and rationalized by DFT calculations. In the case of azaborine **7a** conformational studies by diffraction X-ray was performed. The 3D-disposition of the conformation *anti*-(+61°) of azaborine **7a** found by DFT optimizations is very similar to the crystalline structure investigated and this prove the reliability of calculations.

Atropisomers of azaborine **13** was resolved by Chiralpak AS-H column, and subsequently, kinetic analysis was performed in order to determine free energy barrier to racemization ($\Delta G^{\neq}$ = 32.8 kcal/mol).
The absolute configuration of the two atropisomers was assigned by comparison of the experimental ECD spectra acquired at +25 °C of the enantiomers with simulated ECD spectra. At the first eluted and second eluted atropisomer was assigned respectively *M* and *P* absolute configuration.

Isosteric compound **21** was synthesized and used as reference standard. By DFT calculations was found that $\Delta G^{\neq}$ corresponding to the rotation of aryl group is higher than $\Delta G^{\neq}$ of rotational process of benzyl moiety, that is the opposite experimental trend regard the azaborine **7a**. A plausible explanation of this theoretical prediction is that B-C_{aryl} (**7a**) is longer than C_{naphth}-C_{aryl} (**21**) and for this reason the energy barrier raises because the aryl substituent might be closer to naphthalene framework but also a different electronic effect must be considered. Future conformational studies on compound **22** should allow to assign by comparison the relative energy barriers to the respective axes and to get further data.

5. Experimental section

5.1 Materials

2′-Aminoacetophenone, 4-Nitrobenzyl bromide, m-Tolyl boronic acid, 2-Naphthol, 1-Bromo-2-methylnaphthalene, 4-Nitrobenzaldehyde and 2,3-dimethylphenyl boronic acid were commercially available. Et2O has been dried before use by distillation from Na/benzophenone and Toluene had been dried on molecular sieves. The deuterated solvents for NMR spectra were commercially available; CDFCl2 had been prepared in this laboratory[30] before this thesis work started.

5.2 Instrumentations

The following stationary phases were employed for the chromatography: Silica gel 60 F254 (Merck) for the TLC and silica gel 60 Å (230-400 mesh, Sigma Aldrich) for atmospheric pressure chromatography.

Reactions which needed anhydrous conditions were performed under dried nitrogen flow (inert atmosphere). The glassware used in these reactions was placed in an oven at +70 °C for at least 3 hours immediately before use.

To purify the products, a HPLC Waters[TM] 600 instrument with detection fixed at 254 nm was used. Phenomenex Luna C18 (5 μm 250x21.2 mm, 20 mL/min) semipreparative column was used to purify the compounds using mixtures of acetonitrile and water as eluent.

Enantioselective HPLC columns (Chiralpak AS-H 5μm 250×4.6 mm, 1.1 mL/min and DAICEL Chiralcel AD-H column 5 μm, 250x21.2 mm, 20 ml/min) have been used to separate the stable atropisomers, using mixtures of hexane and isopropanol as eluents.

^{1}H-NMR, ^{13}C-NMR and ^{19}F-NMR spectra were registered with a Varian Inova 600 MHz and a Varian Mercury 400 MHz spectrometer. Chemical shifts are given in ppm relative to the internal standards tetramethylsilane (^{1}H and ^{13}C) or relative to the residual peak of the solvents. Assignment of the carbons multiplicity were obtained by means of the DEPT sequences.

The low temperature spectra were obtained by using a flow of dry nitrogen which entered into a inox steel heat-exchanger immersed in liquid nitrogen and connected to the NMR probe head by a vacuum-insulated transfer line. Temperature calibrations were performed before the experiments, using a digital thermometer and a Cu/Ni

thermocouple placed in an NMR tube filled with isopentane (for low temperature calibration) or with tetrachloroethane (for high temperature calibration). The uncertainty in the temperature measurements can be estimated from the calibration curve as ±1 °C.

Lineshape simulations were performed using a PC version of the QCPE DNMR6 program.[31] Electronic superimposition of the original and the simulated spectra enabled the determination of the most reliable rate constants at few different temperatures. These constants provided the free energies of activation ($\Delta G^{\#}$) by means of the Eyring equation.[32] Within the experimental uncertainty, the latter values were found essentially invariant in the examined temperature range, thus implying an almost negligible activation entropy ($\Delta S^{\#}$), as observed in the majority of conformational processes investigated by dynamic NMR.[33]

ECD spectra were recorded with a JASCO J-810 spectropolarimeter at +25 °C in acetonitrile solutions. The concentrations of the samples were tuned to obtain a maximum absorbance of about 0.9-1.0 in the UV spectrum, using a quartz cell with 0.2 cm path length. Spectra were recorded in the 190-400 nm interval.

5.3 Calculations

A conformational search was preliminarily carried out by means of the molecular mechanics force field (MMFF), using the package ComputeVOA 0.1.[34] The most stable conformers thus identified were subsequently energy minimized by DFT computations, which were performed by the Gaussian 09, rev. D.01, series of programs using standard optimization parameters.[35] The calculations for ground states and transition states employed the B3LYP hybrid HF-DFT method and the 6-31G(d) basis sets. The analysis of the vibrational frequencies for every optimized structure has shown the absence of imaginary harmonic frequencies for the ground states, and the presence of a single imaginary frequency for the transition states. Visual inspection of the corresponding normal mode[36] validated the identification of the transition states.

The ECD spectra were simulated by means of TD-DFT calculations. The electronic excitation energies and rotational strengths have been calculated in the gas phase using the geometries obtained at the B3LYP/6-31G(d) level with the CAM-B3LYP functional. All the calculations employed the 6-311++G(2d,p) basis set because this basis set has been widely used in this kind of calculation and proved to be sufficiently accurate at a

reasonable computational cost. The simulated spectra were obtained using the first 60 calculated transitions (lowest wavelength about 180 nm) and applying a 0.25 eV line width. The simulated spectra resulting from the Boltzmann averaged sum of the conformations were red-shifted by 10 nm to get the best simulations with the experimental spectra.

5.4 Synthesis

The two 1,2-azaborines **7a** and **7b** were prepared following the general synthetic scheme reported below:
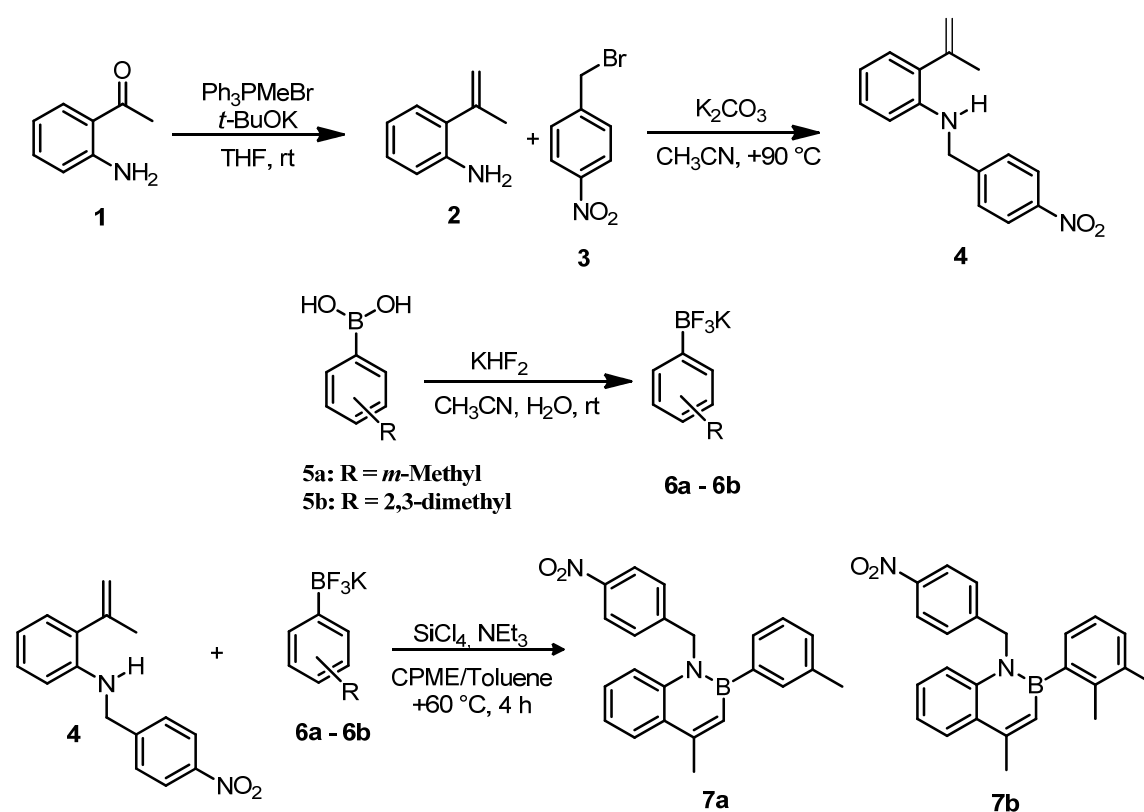
Synthesis of 2-(prop-1-en-2-yl)aniline (**2**)
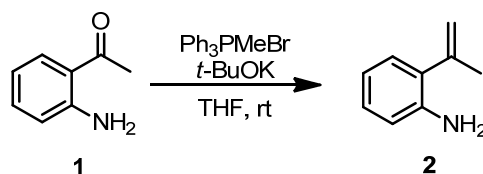
To a solution of Ph$_3$PMeBr (11.89 g, 33.15 mmol, 1.5 eq) in dry THF (100 mL) was added *t*-BuOK (3.72 g, 33.15 mmol, 1.5 eq) in two portions under N$_2$ atmosphere at room

temperature. After the mixture was stirred at room temperature for 30 min, a solution of **1** (3.00 g, 22.21 mmol, 1 eq) in dry THF (120 mL) was added dropwise. The reaction mixture was then stirred at room temperature under N_2 overnight. The reaction mixture was quenched with H_2O (100 mL), concentrated and extracted twice with EtOAc (100 mL x 2). The combined organic layers were washed with saturated $NaHCO_3$ and brine, dried over Na_2SO_4, filtered and concentrated. Fractional distillation under vacuum conditions of the residue gave **2** with b.p. +87 °C / 9 mbar. The product was obtained with a 76 % yield (2.31 g) as a pale yellow liquid.

Spectroscopic data of 2-(prop-1-en-2-yl)aniline (**2**)

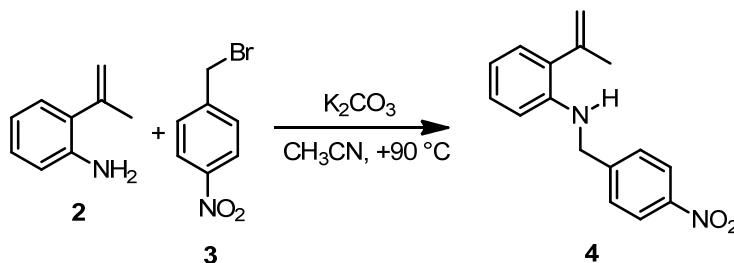**^{1}H-NMR** (600 MHz, CDCl$_3$, TMS, +25 °C) : δ 2.07 (s, 3H); 3.82 (bs, 2H); 5.06 (bs, 1H); 5.29 (bs, 1H); 6.70 (d, *J* = 8.1 Hz, 1H); 6.73 (dd, J_1 = 7.3 Hz, J_2 = 7.3 Hz, 1H); 7.01 - 7.08 (m, 2H).

^{13}C-NMR (150.8 MHz, CDCl$_3$, 77.0 ppm, +25 °C) : δ 23.8 (CH$_3$); 115.3 (CH$_2$); 115.5 (CH); 118.2 (CH); 127.9 (CH); 128.2 (CH); 139.2 (Cq); 142.8 (Cq); 143.4 (Cq).

Synthesis of N-(4-nitrobenzyl)-2-(prop-1-en-2-yl)aniline (**4**)

To a solution of **2** (2.02 g, 15.16 mmol, 1 eq) in CH$_3$CN (100 mL) was added K$_2$CO$_3$ (4.19 g, 30.33 mmol, 2 eq) at room temperature, followed by solution of **3** (3.28 g, 15.16 mmol, 1 eq) in CH$_3$CN (200 mL). The reaction mixture was heated to +90 °C and stirred overnight. After cooling to rt, the reaction was quenched with water (200 mL). The aqueous layer was extracted by EtOAc (200 mL x 3) and combined organic layers were dried over Na$_2$SO$_4$. After removing the solvent, the residue was purified by column chromatography (Hexane : EtOAc = 11 : 1 with 1% NEt$_3$) to afford the product as an orange solid with a 47 % yield (1.88 g).

Spectroscopic data of N-(4-nitrobenzyl)-2-(prop-1-en-2-yl)aniline (4)

^{1}H-NMR (600 MHz, CDCl$_3$, TMS, +25 °C) : δ 2.09 (bs, 3H); 4.46 (s, 2H); 4.73 (bs, 1H); 5.09 (bs, 1H); 5.34 (bs, 1H); 6.43 (d, J = 8.5 Hz, 1H); 6.70 (dd, J_1 = 7.5 Hz, J_2 = 7,5 Hz, 1H); 7.02 – 7.07 (m, 2H); 7.48 (m, 2H); 8.16 (m, 2H).

^{13}C-NMR (150.8 MHz, CDCl$_3$, 77.0 ppm, +25 °C) : δ 24.1 (CH$_3$); 47.5 (CH$_2$); 110.5 (CH); 115.9 (CH$_2$); 117.4 (CH); 123.8 (CH); 127.5 (CH); 127.9 (CH); 128.0 (CH); 129.5 (Cq); 143.2$_7$ (Cq); 143.3$_0$ (Cq); 147.0 (Cq); 147.6 (Cq).

Synthesis of potassium *m*-tolyltrifluoroborate (6a)

5a → 6a
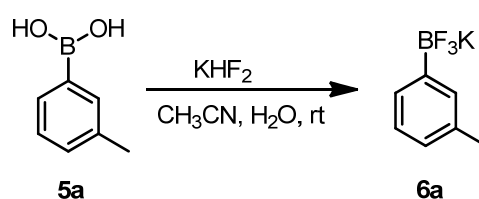
To a solution of corresponding boronic acid **5a** (100 mg, 0.74 mmol, 1 eq) dissolved in CH$_3$CN (0.22 mL) was added slowly with vigorous stirring a solution of KHF$_2$ (191.3 mg, 2.45 mmol, 3.33 eq) in H$_2$O (0.54 mL). The resulting mixture was stirred for 15 min and white solid was obtained, CH$_3$CN and H$_2$O was removed as azeotropic mixture CH$_3$CN/H$_2$O under reduced pressure. The yield is almost quantitative (138.2 mg).

Spectroscopic data of potassium *m*-tolyltrifluoroborate (6a)

^{1}H-NMR (600 MHz, CD$_3$CN, 1.96 ppm, +25 °C) : δ 2.31 (s, 3H); 6.98 (d, J = 7.1 Hz, 1H); 7.10 (dd, J_1 = 7.1 Hz, J_2 = 7.1 Hz, 1H); 7.27 (d, J = 7.1 Hz, 1H); 7.32 (s, 1H).

^{13}C-NMR (150.8 MHz, CD$_3$CN, 118.3 ppm, +25 °C) : δ 21.6 (CH$_3$); 127.3 (CH); 127.6 (CH); 129.2 (CH); 133.0 (CH); 136.5 (Cq); 148.4 (b, B-Cq).

^{19}F-NMR (564.3 MHz, CD$_3$CN, C$_6$F$_6$, -163 ppm, +25 °C) : δ -142.2 (J = 40 Hz, BF$_3$).

Synthesis of potassium 2,3-dimethylphenylltrifluoroborate (6b)

5b → 6b

To a solution of corresponding boronic acid **5b** (250 mg, 1.67 mmol, 1 eq) dissolved in CH$_3$CN (0.5 mL) was added slowly with vigorous stirring a solution of KHF$_2$ (433.2 mg, 5.54 mmol, 3.33 eq) in H$_2$O (1.2 mL). The resulting mixture was stirred for 15 min and white solid was obtained, CH$_3$CN and H$_2$O was removed as azeotropic mixture CH$_3$CN/H$_2$O under reduced pressure. The yield is almost quantitative (350.1 mg).
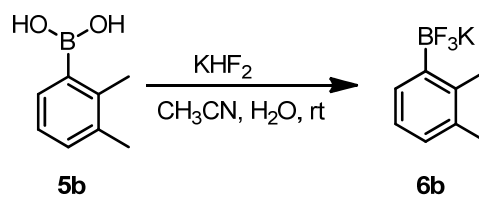
Spectroscopic data of potassium 2,3-dimethylphenylltrifluoroborate (**6b**)

^{1}H-NMR (600 MHz, CD$_3$CN, 1.96 ppm, +25 °C) : δ 2.22 (s, 3H); 2.31 (s, 3H); 6.86 – 6.92 (m, 2H); 7.3 (d, J = 6.6 Hz, 1H).

^{13}C-NMR (150.8 MHz, CD$_3$CN, 118.3 ppm, +25 °C) : δ 18.2 (CH$_3$); 20.6 (CH$_3$); 124.7 (CH); 128.2 (CH); 130.7 (CH); 135.7 (Cq); 140.5 (Cq); 148.0 (b, B-Cq).

^{19}F-NMR (564.3 MHz, CD$_3$CN, C$_6$F$_6$, -163 ppm, +25 °C) : δ -139.0 (J = 41 Hz, BF$_3$).

Synthesis of 4-methyl-1-(4-nitrobenzyl)-2-(m-tolyl)-1,2-dihydrobenzo[e][1,2]azaborinine (**7a**)
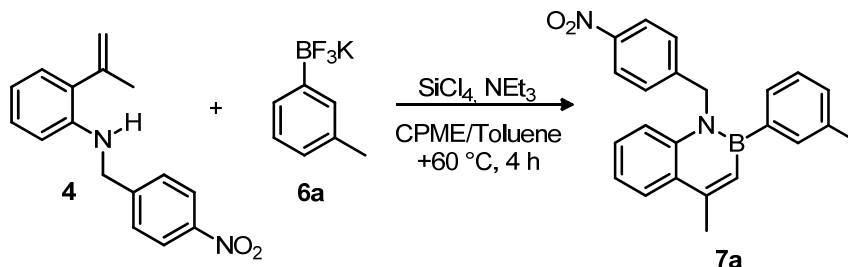
In a vial equipped with a stirring bar were added potassium organotrifluoroborate **6a** (50 mg, 0.25 mmol, 1 eq) and amine **4** (81.1 mg, 0.30 mmol, 1.2 eq) dissolved in mixture of cyclopentyl methyl ether/toluene (0.25 mL : 0.25 mL) under nitrogen atmosphere. Subsequently, were added SiCl$_4$ (29 µL, 0.25 mmol, 1 eq), NEt$_3$ (26 µL, 0.19 mmol, 0.75 eq) and the resulting mixture was heated to +60 °C for 4 h. After cooling to ambient temperature, the reaction mixture was diluited with hexane and it was passed through a silica gel plug (10 mL CH$_2$Cl$_2$) to remove the impurities. Then, the solvent was removed under reduced pressure and the residue was purified by chromatography column (hexane : CH$_2$Cl$_2$ = 8 : 2 with 1% of NEt$_3$). The product **7a** was collected as a pale yellow oil with a 62 % yield (57.6 mg).

Spectroscopic data of 4-methyl-1-(4-nitrobenzyl)-2-(m-tolyl)-1,2-dihydrobenzo[e][1,2]azaborinine (**7a**)

^{1}H-NMR (600 MHz, CD$_2$Cl$_2$, 5.33 ppm, +25 °C) : δ 2.32 (s, 3H); 2.70 (bs, 3H); 5.52 (s, 2H); 6.89 (bs, 1H); 7.17 (d, J = 7.6 Hz, 1H); 7.21 – 7.32 (m, 6H); 7.34 (s, 1H); 7.38 (ddd, J_1 = 8.4 Hz, J_2 = 7.0 Hz, J_3 = 1.5 Hz, 1H); 7.97 (dd, J_1 = 8.1 Hz, J_2 = 1.5 Hz, 1H); 8.14 (m, 2H).

^{13}C-NMR (150.8 MHz, CD$_2$Cl$_2$, 53.8 ppm, +25 °C) : δ 21.6 (CH$_3$); 23.2 (CH$_3$); 52.4 (CH$_2$); 117.2 (CH); 121.5 (CH); 124.3 (CH); 126.9 (CH); 127.1 (CH); 127.8 (Cq); 128.0 (CH); 128.7 (CH); 129.1 (CH); 129.5 (CH); 132.0 (b, B-CH); 133.5 (CH); 137.6 (Cq); 141.1 (Cq); 142.1 (b, B-Cq); 147.4 (Cq); 147.8 (Cq); 152.0 (Cq).

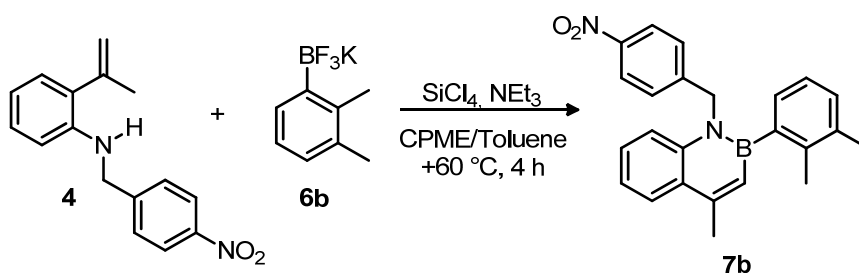Synthesis of 2-(2,3-dimethylphenyl)-4-methyl-1-(4-nitrobenzyl)-1,2-dihydrobenzo[e][1,2]azaborinine (**7b**)

In a vial equipped with a stir bar were added in order potassium organotrifluoroborate **6b** (50.1 mg, 0.24 mmol, 1 eq) and amine **4** (75.8 mg, 0.28 mmol, 1.2 eq) dissolved in mixture of cyclopentyl methyl ether/toluene (0.25 mL : 0.25 mL) under nitrogen atmosphere. Subsequently, were added SiCl$_4$ (29 µL, 0.25 mmol, 1 eq), NEt$_3$ (26 µL, 0.19 mmol, 0.75 eq) and the resulting mixture was heated to 60 °C for 4 h. After cooling to ambient temperature, the reaction mixture was diluited with hexane and it was passed through a silica gel plug (10 mL CH$_2$Cl$_2$) to remove the impurities. Then, the solvent was removed under reduced pressure and the residue was purified by chromatography column (hexane : CH$_2$Cl$_2$ = 8 : 2 with 1% of NEt$_3$). The product **7b** was collected as a pale yellow oil with a 41 % yield (37.0 mg).

Spectroscopic data of 2-(2,3-dimethylphenyl)-4-methyl-1-(4-nitrobenzyl)-1,2-dihydrobenzo[e][1,2]azaborinine (**7b**)

^{1}**H-NMR** (600 MHz, CDCl$_3$, TMS, +25 °C) : δ 2.17 (s, 3H); 2.27 (s, 3H); 2.66 (bs, 3H); 5.30 (d, J = 17.5 Hz, 1H); 5.35 (d, J = 17.5, 1H); 6.79 (bs, 1H); 7.00 – 7.06 (m, 2H); 7.10 (dd, J_1 = 6.9 Hz, J_2 = 2.2 Hz, 1H); 7.15 – 4.20 (m, 3H); 7.23 – 7.27 (m, 1H); 7.34 (ddd, J_1 = 8.6 Hz, J_2 = 7.3 Hz, J_3 = 1.7 Hz, 1H); 7.94 (dd, J_1 = 8.2 Hz, J_2 = 1.6 Hz, 1H); 8.08 (m, 2H).

^{13}**C-NMR** (150.8 MHz, CDCl$_3$, 77.0 ppm, +25 °C) : δ 20.2 (2CH$_3$); 23.0$_5$ (CH$_3$); 51.8 (CH$_2$); 116.7 (CH); 121.2 (CH); 123.8 (CH); 125.2 (CH); 126.6 (CH); 126.7 (CH); 127.5 (Cq); 128.2 (CH); 128.4 (CH); 129.3 (CH); 131.6 (b, B-CH); 136.3 (Cq); 137.6 (Cq); 140.6 (Cq); 142.2 (b, B-Cq); 146.8 (Cq); 146.9 (Cq); 151.1 (Cq).

Synthesis of the third sterically hindered 1,2-azaborine was carried out as follow:
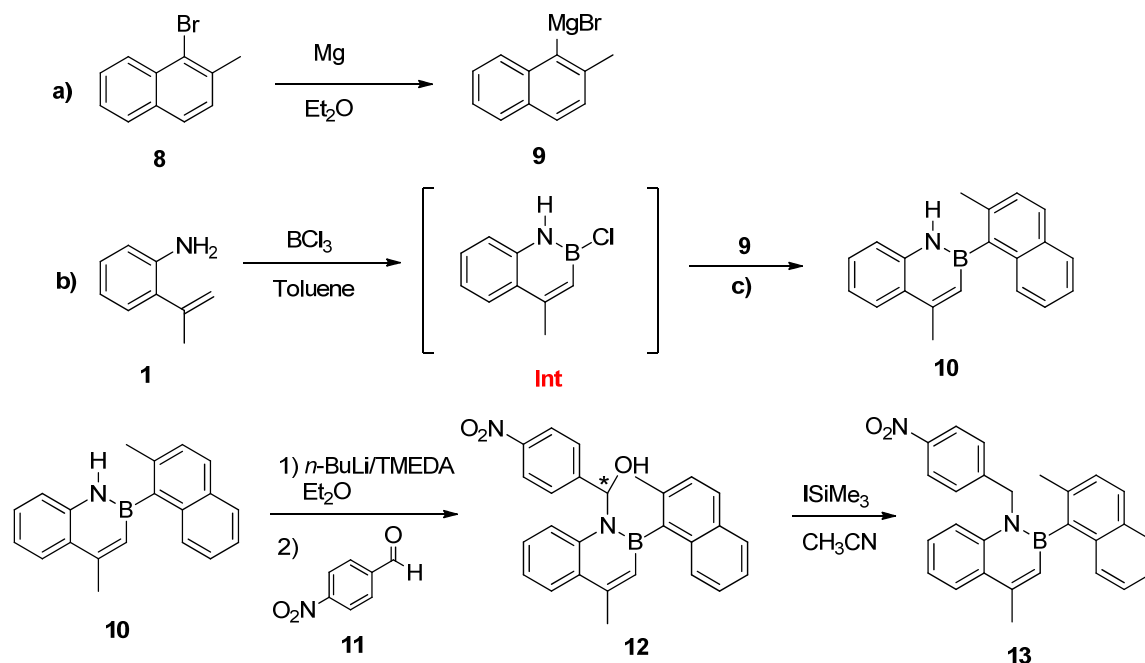
Synthesis of 4-methyl-2-(2-methylnaphthalen-1-yl)-1,2-dihydrobenzo[e][1,2]azaborinine (**10**)

Three-steps synthesis

a) Preparation of Grignard reagent

Under dried nitrogen, magnesium (210.5 mg, 8.66 mmol, 5.5 eq) was put in a round bottomed flask with 20 mL of anhydrous Et$_2$O and I$_2$ was used as catalyst and indicator.

1-bromo-2-methylnaphthalene (1.34 mL, 8.66 mmol, 5.5 eq) was then added dropwise and then was warmed up to reflux for 30 min. The reaction mixture was orange before the addition of **8**, decoloured when the reaction started, and became milky with the formation of the Grignard reagent.

b) Preparation of the 2-chloro-2,1-borazaronapthalene (Intermediate)

Under nitrogen atmosphere, a solution 1 M of boron trichloride in hexane (3.4 mL, 2.27 eq) was added dropwise to the stirred solution of the amine (200.6 mg, 1.50 mmol, 1 eq) in anhydrous toluene (10 mL). The dark orange reaction mixture was heated to reflux for 1h.

c) Nucleophilic substitution

Grignard reagent was added dropwise via cannula to the previous solution cooled to room temperature. The obtained mixture was then heated to reflux for another hour. After cooling to ambient temperature the reaction was quenched with water (10 mL) and the mixture was extracted with Et_2O (50mLx3). The combined organic layers were dried over Na_2SO_4, filtered, concentrated under reduce pressure and purified by chromatography column (petroleum ether 100 % with gradient to EP : CH_2Cl_2 = 7 : 3). Product **10** was collected as a white solid with a 75 % yield (320.4 mg).

Spectroscopic data of 4-methyl-2-(2-methylnaphthalen-1-yl)-1,2-dihydrobenzo[e][1,2]azaborinine (**10**)

^{1}H-NMR (400 MHz, CD_3CN, 1.96 ppm, +25 °C) : δ 2.42 (s, 3H); 2.67 (d, J = 1.1 Hz, 3H); 6.82 (q, J = 1.1 Hz, 1H); 7.28 (ddd, J_1 = 8.3 Hz, J_2 = 6.7 Hz, J_3 = 1.6 Hz, 1H); 7.31 (ddd, J_1 = 8.5 Hz, J_2 = 6.9 Hz, J_3 = 1.6 Hz, 1H); 7.38 (ddd, J_1 = 8.1 Hz, J_2 = 6.7 Hz, J_3 = 1.2 Hz, 1H); 7.40 (d, J = 8.4 Hz, 1H); 7.46 (td, J_1 = J_2 = 8.2 Hz, J_3 = 1.5 Hz, 1H); 7.49 (ddd, J_1 = 8.1 Hz, J_2 = 6.8 Hz, J_3 = 1.5 Hz, 1H); 7.65 (d, J = 8.4 Hz, 1H); 7.80 (d, J = 8.4, 1H); 7.85 (d, J = 8.2, 1H); 7.96 (d, J = 8.2, 1H); 8.87 (bs, 1H).

^{13}C-NMR (100.5 MHz, CD_3CN, 118.3 ppm, +25 °C) : δ 23.1 (CH_3); 23.3 (CH_3); 119.8 (Cq); 122.0 (CH); 125.4 (CH); 126.1$_6$ (Cq); 126.1$_8$ (CH); 126.7 (CH); 128.4 (CH); 129.0 (CH); 129.2 (CH); 129.4 (CH); 129.5 (CH); 131.8 (b, B-CH); 132.5 (CH); 137.1 (Cq); 138.6 (Cq); 140.0 (b, B-Cq); 142.0 (Cq); 152.3 (Cq).

Synthesis of (4-methyl-2-(2-methylnaphthalen-1-yl)benzo[e][1,2]azaborinin-1(2h)-yl)(4-nitrophenyl)methanol (**12**)
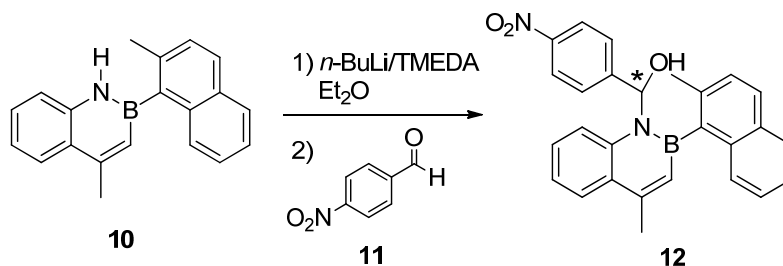
To a solution of **10** (70.0 mg, 0.247 mmol, 1 eq) in dry Et_2O (20 mL) was added TMEDA (0.11 mL, 0.742 mmol, 3 eq) under nitrogen atmosphere. Then, a solution of *n*-BuLi 1.6 M in hexane (0.46 mL, 0.742 mmol, 3 eq) was dropped at 0 °C with vigorous stirring. The reaction mixture was stirred for 1 h and after warming to room temperature *p*-nitro-benzaldehyde (186.8 mg, 1.24 mmol, 5 eq) was added and the mixture was stirred for two hours. Saturated solution of NH_4Cl (10 mL) was added to quench reaction and after extraction with Et_2O (50mLx3), drying over Na_2SO_4, filtration and evaporation under reduced pressure of the solvent, two diastereoisomers were purified by silica column chromatography (petroleum ether : Et_2O = 9 : 1 → 6 : 4) and isolated with semipreparative HPLC on a Luna C18 column (10 μm, 100 Å, 250 x 21.20 mm, 20 mL/min, CH_3CN : H_2O = 9 : 1). The products **12** were collected as a white solids in a 37 % yield (20.1 mg each diastereoisomer) and unreacted starting material **10** was recovered. The enantiomers of each diastereoisomer were resolved on DAICEL Chiralcel AD-H column (5 μm, 250x21.2 mm, 20 ml/min, hexane : *i*-PrOH = 8 : 2).

Spectroscopic data

Ritention time of diastereoisomer 1= 10.4 min

^{1}H-NMR (600 MHz, CD_3CN, 1.96 ppm, +25 °C) : δ 2.48 (s, 3H); 2.70 (s, 3H); 5.27 (bs, 1H); 6.67$_5$ (bs, 1H); 6.80 (s, 1H); 7.18 - 7.27 (m, 2H); 7.28 - 7.33 (m, 1H); 7.33 - 7.37 (m, 1H); 7.45 (d, *J* = 8.5 Hz, 1H); 7.49 (m, 2H); 7.54 (dd, J_1 = 8.5 Hz, J_2 = 0.9 Hz, 1H); 7.70 (d, *J* = 8.3 Hz, 1H); 7.79 - 7.84 (m, 2H); 8.00 - 8.04 (m, 3H).

^{13}C-NMR (150.8 MHz, CD_3CN, 118.3 ppm, +25 °C) : δ 23.3 (CH_3); 23.5 (CH_3); 84.0 (CH); 122.5 (CH); 124.3 (CH); 125.7 (CH); 126.4 (CH); 127.5 (CH); 128.0$_1$ (CH); 128.0$_4$ (CH); 128.6 (CH); 129.1 (Cq); 129.2 (CH); 129.4 (CH); 129.6 (CH); 131.7 (b, B-

CH); 132.5 (Cq); 136.3 (Cq); 138.5 (Cq); 139.8 (b, B-Cq); 140.0 (Cq); 148.2 (Cq); 150.7 (Cq); 153.4 (Cq).

Ritention time of diastereoisomer 2 = 12.7 min

^{1}H-NMR (600 MHz, CD$_3$CN, 1.96 ppm, +25 °C) : δ 2.41 (s, 3H); 2.68 (bs, 3H); 4.89 (bs, 1H); 6.71 (bs, 1H); 6.79 (s, 1H); 7.18 - 7.26 (m, 2H); 7.33 (d, J = 8.4 Hz, 1H); 7.38 - 7.46 (m, 4H); 7.56 (dd, J_1 = 8.4 Hz, J_2 = 1.1 Hz, 1H); 7.60 (d, J = 8.2 Hz, 1H); 7.79 (d, J = 8.4 Hz, 1H); 7.87 (d, J = 8.1 Hz, 1H); 8.01 (dd, J_1 = 8.0 Hz, J_2 = 1.8 Hz, 1H); 8.06 (m, 2H).

^{13}C-NMR (150.8 MHz, CD$_3$CN, 118.3 ppm, +25 °C) : δ 23.3 (CH$_3$); 23.8 (CH$_3$); 84.2 (CH); 122.5 (CH); 124.4 (CH); 125.8 (CH); 126.9 (CH); 127.5 (CH); 127.9 (CH); 128.0 (CH); 128.6 (CH); 129.1$_7$ (Cq); 129.1$_8$ (CH); 129.3 (CH); 129.4 (CH); 131.8 (b, B-CH); 132.6 (Cq); 136.4 (Cq); 138.3 (Cq); 139.7 (b, B-Cq); 139.9 (Cq); 148.3 (Cq); 150.5 (Cq); 153.5 (Cq).

Synthesis of 4-methyl-2-(2-methylnaphthalen-1-yl)-1-(4-nitrobenzyl)-1,2-dihydrobenzo[e][1,2]azaborinine (**13**)
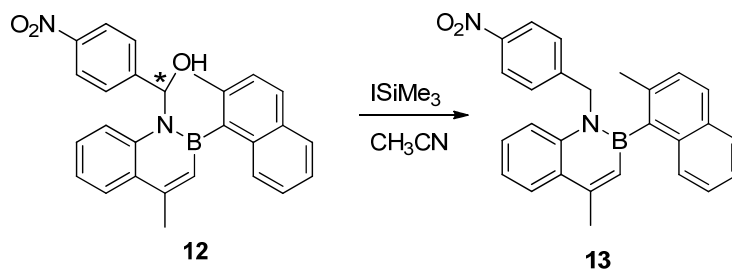
To a solution of **12** (16.1 mg, 0.0370 mmol, 1 eq) in CH$_3$CN (3 mL) was dropped ISiMe$_3$ (d = 1.47 g/mL, 30 µL, 0.222 mmol, 6 eq) under nitrogen atmosphere. The mixture was stirred for 24 h at room temperature. Diluition with water (10 mL), extraction with Et$_2$O (20 mL x 3), subsequent plug on silica gel and purification with semipreparative HPLC on Luna C18 column (10 µm, 100 Å, 250 x 21.20 mm, 20 mL/min, CH$_3$CN : H$_2$O = 9 : 1) gave the product **13** with 80 % of yield (12.4 mg). The atropisomeric pair of the product was resolved on Chiralpak AS-H column (5µm, 250×4.6 mm, 1.1 mL/min, hexane : i-PrOH = 9 :1).

Spectroscopic data of 4-methyl-2-(2-methylnaphthalen-1-yl)-1-(4-nitrobenzyl)-1,2-dihydrobenzo[e][1,2]azaborinine (13)

¹H-NMR (600 MHz, CDCl₃, TMS, +25 °C) : δ 2.30 (s, 3H); 2.70 (bs, 3H); 5.24 (d, J = 17.5 Hz, 1H); 5.28 (d, J = 17.5 Hz, 1H); 6.86 (s, 1H); 7.11 (m, 2H); 7.24 (d, J = 8.5 Hz, 1H); 7.25 - 7.28 (m, 1H); 7.28 - 7.33 (m, 2H); 7.34 - 7.37 (m, 1H); 7.37 - 7.41 (m, 1H); 7.50 (d, J = 8.4 Hz, 1H); 7.73 (d, J = 8.4 Hz, 1H); 7.80 (d, J = 8.2 Hz, 1H); 7.98 - 8.03 (m, 3H).

¹³C-NMR (150.8 MHz, CDCl₃, 77.0 ppm, +25 °C) : δ 23.0 (CH₃); 23.1 (CH₃); 51.9 (CH₂); 116.8 (CH); 121.4 (CH); 123.7 (CH); 124.6 (CH); 125.5 (CH); 126.7 (CH); 126.8 (CH); 127.6 (Cq); 127.7 (CH); 128.0 (CH); 128.2₆ (CH); 128.2₇ (CH); 128.5 (CH); 131.5 (Cq); 131.9 (b, B-CH); 135.2 (Cq); 137.1 (Cq); 138.9 (b, B-Cq); 141.0 (Cq); 146.5 (Cq); 146.8 (Cq); 151.4 (Cq).

Synthesis of the corresponding isosteric compound **21**:

45
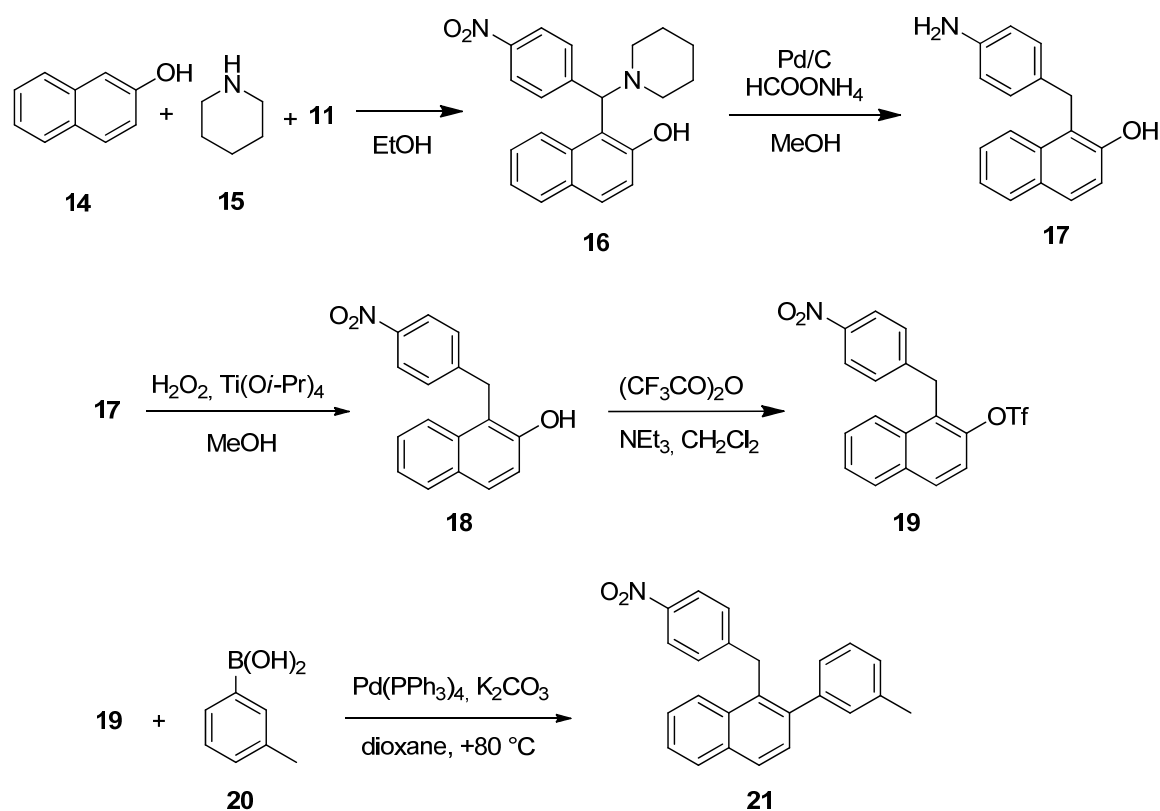
Synthesis of 1-((4-nitrophenyl)(piperidin-1-yl)methyl)naphthalen-2-ol (16)
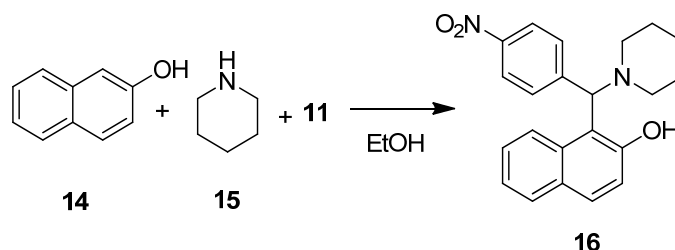
To a solution of β-naphtol **14** (1.44 g, 10 mmol, 1eq) in EtOH (20 mL) were added in sequence piperidine **15** (d = 0.862 g/mL, 1.0 mL, 1 eq) and *p*-nitrobenzaldehyde **11** (1.51 g, 10 mmol, 1eq) and the mixture was stirred at reflux for 12h. After cooling to rt the solvent was removed under reduced pressure and **16** was precipitated by addition of MeOH. The product was collected as a yellow solid with 80 % yield (2.90 g).

Spectroscopic data of 1-((4-nitrophenyl)(piperidin-1-yl)methyl)naphthalen-2-ol (16)

^{1}H-NMR (600 MHz, CDCl$_3$, TMS, +25 °C) : δ 1.29 (bs, 1H); 1.44 - 1.88 (m, 5H); 1.99 (bs, 1H); 2.13 (bs, 1H); 2.64 (bs, 1H); 3.35 (bs, 1H); 5.20 (s, 1H); 7.17 (d, *J* = 8.9 Hz, 1H); 7.23 – 7.27 (m, 1H); 7.40 (ddd, J_1 = 8.3 Hz, J_2 = 6.9 Hz, J_3 = 1.2 Hz, 1H); 7.69 (d, *J* = 8.9 Hz, 1H); 7.72 (d, *J* = 8.0 Hz, 1H); 7.77 (bs, 2H); 7.79 (d, *J* = 8.6 Hz, 1H); 8.12 (d, *J* = 8.5 Hz, 2H); 13.61 (s, 1H).

^{13}C-NMR (150.8 MHz, CDCl$_3$, 77.0 ppm, +25 °C) : δ 24.0 (CH$_2$); 25.9 (b, CH$_2$); 52.3 (b, CH$_2$); 54.6 (b, CH$_2$); 71.1 (CH); 114.9 (Cq); 120.0 (CH) 120.4 (CH); 122.7 (CH); 124.1 (b, CH); 126.7 (CH); 128.7 (b, Cq); 129.1 (CH); 129.7 (b, CH); 130.1 (CH); 132.0 (Cq); 147.3 (Cq); 147.4 (Cq); 155.4 (Cq).

Synthesis of 1-(4-aminobenzyl)naphthalen-2-ol (17)
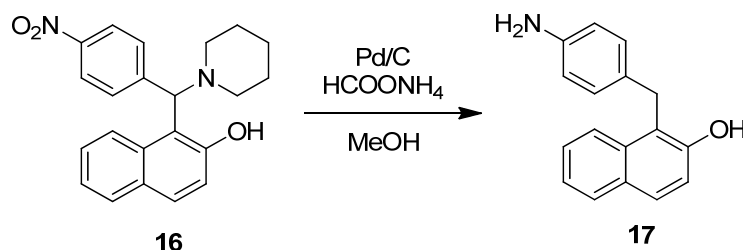
To a mixture of the Mannich base **16** (1.00 g, 2.76 mmol, 1 eq) in MeOH (60 mL) were added ammonium formiate (0.70 g, 11.04 mmol, 4 eq) and Pd/C (160 mg, cat). The

reaction mixture was stirred at reflux for 12 h and after cooling to rt it was filtered on a decalite bed to remove the catalyst. The solvent was removed under reduced pressure and the residue was extracted with EtOAc (100 mL x 3). The organic phase was washed twice with saturated solution of NH$_4$Cl (100 mL x 2) and dried over Na$_2$SO$_4$. Subsequent isolation by chromatography column (petroleum ether : EtOAc = 6 : 4) gave the product **17** as a light pink solid with 95 % yield (657.4 mg).

Spectroscopic data of 1-(4-aminobenzyl)naphthalen-2-ol (**17**)

^{1}H-NMR (600 MHz, CD$_3$CN, 1.96 ppm, +25 °C) : δ 3.92 (bs, 2H); 4.27 (s, 2H); 6.51 (m, 2H); 6.93 (m, 2H); 7.09 (bs, 1H); 7.21 (d, *J* = 8.8 Hz, 1H); 7.29 (ddd, *J*$_1$ = 8.0 Hz, *J*$_2$ = 6.9 Hz, *J*$_3$ = 1.0 Hz, 1H); 7.41 (ddd, *J*$_1$ = 8.3 Hz, *J*$_2$ = 6.9 Hz, *J*$_3$ = 1.3 Hz, 1H); 7.70 (d, *J* = 8.8 Hz, 1H); 7.80 (d, *J* = 8.2 Hz, 1H); 7.91 (d, *J* = 8.5 Hz, 1H).

^{13}C-NMR (150.8 MHz, CD$_3$CN, 118.3 ppm, +25 °C) : δ 30.1 (CH$_2$); 115.5 (CH); 118.9 (CH); 120.2 (Cq); 123.7 (CH); 124.4 (CH); 127.2 (CH); 128.8 (CH); 129.3 (CH); 129.8 (CH); 130.1 (Cq); 130.8 (Cq); 134.6 (Cq); 146.8 (Cq); 152.9 (Cq).

Synthesis of 1-(4-nitrobenzyl)naphthalen-2-ol (**18**)
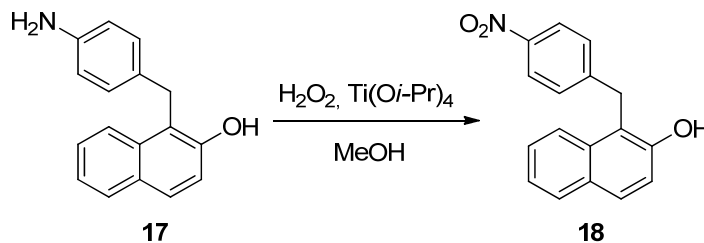
To a solution of the amine **17** (129 mg, 0.517 mmol, 1 eq) in MeOH (15 mL) were added H$_2$O$_2$ 35 % (d= 1.13 g/mL, 300 µL) and Ti(O*i*-Pr)$_4$ (d = 0.96 g/mL, 30 µL, 0.2 eq) in portions. The reaction mixture was stirred at room temperature for 2 h and then water (5 mL) was added to quench reaction. Extraction with CH$_2$Cl$_2$ (20 mL x 3), washing with brine (10 mL), drying over Na$_2$SO$_4$ and subsequence isolation by chromatography column (petroleum ether : Et$_2$O = 6 : 4) gave product **18** as a light brown oil with 48 % yield (70.5 mg).

Spectroscopic data of 1-(4-nitrobenzyl)naphthalen-2-ol (18)

¹H-NMR (400 MHz, CD$_3$CN, 1.96 ppm, +25 °C) : δ 4.54 (s, 2H); 7.26 (d, J = 8.8 Hz, 1H); 7.33 (ddd, J_1 = 8.1 Hz, J_2 = 6.8 Hz, J_3 = 1.2 Hz, 1H); 7.39 (bs, 1H); 7.40 - 7.47 (m, 3H); 7.77 (d, J = 8.9 Hz, 1H); 7.82 - 7.89 (m, 2H); 8.08 (m, 2H).

¹³C-NMR (100.5 MHz, CD$_3$CN, 118.3 ppm, +25 °C) : δ 31.0 (CH$_2$); 118.0 (Cq); 118.8 (CH); 123.8 (CH); 123.9 (CH); 124.3 (CH); 127.6 (CH); 129.5 (CH); 129.7 (CH); 130.1 (CH); 132.5 (Cq); 134.3 (Cq); 147.2 (Cq); 150.6 (Cq); 153.3 (Cq).

Synthesis of 1-(4-nitrobenzyl)naphthalen-2-yl trifluoromethanesulfonate (19)
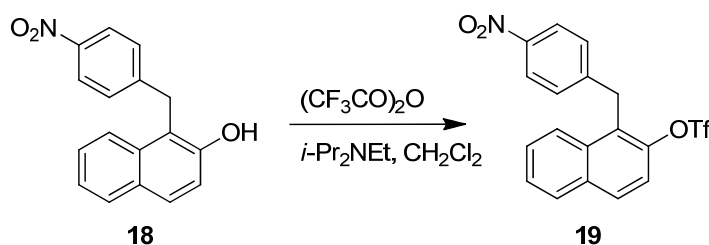
Under nitrogen atmosphere to a solution of naphtol **18** (100.0 mg, 0.358 mmol, 1 eq) in CH$_2$Cl$_2$ (0.8 mL) was added i-Pr$_2$NEt (94 µL, 0.74 g/mL, 1.5 eq) and the solution was cooled to 0 °C. Then triflic anhydride (67 µL, 0.394 mmol, 1.1 eq) was dropped and the reaction mixture was allowed to warp up to room temperature and kept stirred for 12 h. The reaction was quenched by adding of water (15 mL) and washed with aqueous solution of NaHCO$_3$ and HCl and dried over Na$_2$SO$_4$. Concentration of the organic phase and purification by chromatography column (petroleum ether → petroleum ether : Et$_2$O = 8 : 2) gave the pure product **19** as a pale yellow oil in a 32 % yield (47.1 mg).

Spectroscopic data of 1-(4-nitrobenzyl)naphthalen-2-yl trifluoromethanesulfonate (19)

¹H-NMR (400 MHz, CDCl$_3$, TMS, +25 °C) : δ 4.66 (s, 2H); 7.26 (m, 2H); 7.48 (d, J = 9.1 Hz, 1H); 7.52 – 7.60 (m, 2H); 7.83 – 7.88 (m, 1H); 7.91 – 7.97 (m, 2H); 8.1 (m, 2H).

¹³C-NMR (100.5 MHz, CDCl$_3$, 77.0 ppm, +25 °C) : δ 31.7 (CH$_2$); 118.5 (q, J = 319.0 Hz, CF$_3$); 119.5 (CH); 123.8$_5$ (CH); 124.7 (CH); 126.7 (Cq); 127.1 (CH); 128.0$_5$ (CH); 128.9 (CH); 129.0 (CH); 130.3$_5$ (CH); 132.5 (Cq); 132.9 (Cq); 145.8 (Cq); 146.2 (Cq); 146.7 (Cq).

¹⁹F-NMR (376.5 MHz, CDCl$_3$, C$_6$F$_6$, -163 ppm, +25 °C) : δ -73.8 (s, CF$_3$).

Synthesis of 1-(4-nitrobenzyl)-2-(m-tolyl)naphthalene (21)
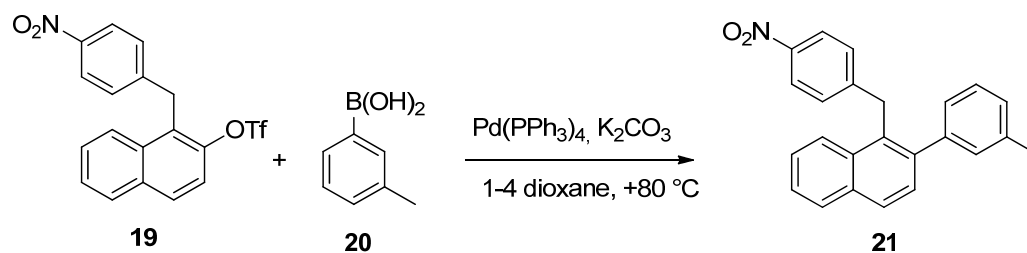
Under nitrogen atmosphere to a solution containing **19** (28.1 mg, 0.068 mmol, 1 eq) and the boronic acid **20** (12.1 mg, 0.89 mmol, 1.3 eq) in dioxane (0.7 mL) were added palladium catalyst (4 mg, 0.05 eq) and aqueous solution of K_2CO_3 2M (102 µL, 0.20 mmol, 3 eq) previously degassed. The reaction mixture was stirred at 80 °C for 2 h in the dark to avoid the oxidation of noble metal. After cooling to room temperature the reaction mixture was passed through a silica gel plug, extracted with EtOAc, washed with brine and water and dried over Na_2SO_4. The solvent was removed under reduced pressure and the product was isolated with semipreparative HPLC on a Luna C18 (10 µm, 100 Å, 250 x 21.20 mm, 20 mL/min, $CH_3CN : H_2O = 95 : 5$). The yield was 62 % (14.9 mg).

Spectroscopic data of 1-(4-nitrobenzyl)-2-(m-tolyl)naphthalene (21)

^{1}H-NMR (600 MHz, CD_2Cl_2, 5.33 ppm, +25 °C) : δ 2.33 (s, 3H); 4.55 (s, 2H); 7.09 (d, J = 7.7 Hz, 1H); 7.11 (s, 1H); 7.16 (m, 2H); 7.19 (d, J = 7.7 Hz, 1H); 7.27 (t, $J_1 = J_2 = 7.6$ Hz, 1H); 7.45 (ddd, $J_1 = 8.4$ Hz, $J_2 = 6.8$ Hz, $J_3 = 1.4$ Hz, 1H); 7.48 - 7.52 (m, 2H); 7.82 (d, $J = 8.5$ Hz, 1H); 7.90 (d, $J = 8.5$ Hz, 1H); 7.94 (d, $J = 8.2$ Hz, 1H); 8.04 (m, 2H).

^{13}C-NMR (150.8 MHz, CD_2Cl_2, 53.8 ppm, +25 °C) : δ 21.5 (CH_3); 35.7 (CH_2); 123.8 (CH); 125.2 (CH); 126.0 (CH); 126.5 (CH); 127.0 (CH); 127.8 (CH); 128.3 (CH); 128.5 (CH); 128.8 (CH); 129.1 (CH); 129.3 (CH); 130.3 (CH); 131.3 (Cq); 132.6 (Cq); 133.7 (Cq); 138.4 (Cq); 141.4 (Cq); 142.3 (Cq); 146.6 (Cq); 150.1 (Cq).

6. Appendix

6.1 Dynamic NMR

Compound that exist as a mixture of fast interconverting stereoisomer are often conveniently viewed, even though inaccurately, as an average structure. A close look reveals that most of organic compounds are conformationally free and for this reason more than one conformers are presents.

Dynamic NMR (DNMR), also called variable-temperature NMR, is a powerful tool used for the investigation stereodynamic processes, making possible by the exhibition of anisochronous nuclei when the interconversion between stereoisomers is slow on the NMR timescale. The resonance frequency of a nucleus is influenced by the magnetic environment and depending on the conformations taken by molecule, the resonance frequencies of some nuclei could be significantly different.

When the conformational motion of a compound is frozen at low temperature, NMR signals relative to the different conformations broaden on warming and eventually coalesce and become a single peak when the conformational exchange becomes very fast on the NMR timescale. This phenomenon occurs when the considered nuclei mutually exchange their position and a single averaged signal is visible. This is the result of a fast rotation along the axis of a bond of the considered molecule.

The mutually exchanging nuclei may give rise to distinct signals only when the difference in chemical shift is big enough to make the lifetime conformations (t), larger than the acquisition time of the spectrum. The equation for the determination of lifetime is

$$t = \frac{\sqrt{2}}{2\pi(\upsilon_A - \upsilon_B)}$$

NMR spectroscopic technique can observe conformational processes that occur in the milliseconds-seconds range.
Two conformations that are not distinguishable by a low field NMR spectrometer could be observed when an high magnetic field because the difference of the signals in Hz is proportional to the applied magnetic field of the spectrometer.
Dynamic NMR approach is useful when the energy barriers are between 4.5 and 21-22 kcal/mol and the range covered by variable-temperature NMR is rather high (from -180

°C to +160 °C) that basically depends on the availability of the deuterated solvent and corresponding boiling and melting points and from the spectrometer limits.

In the Figure 28 is shown the evolution of two signals at low temperature (blue trace) that undergoes to chemical exchange upon heating.
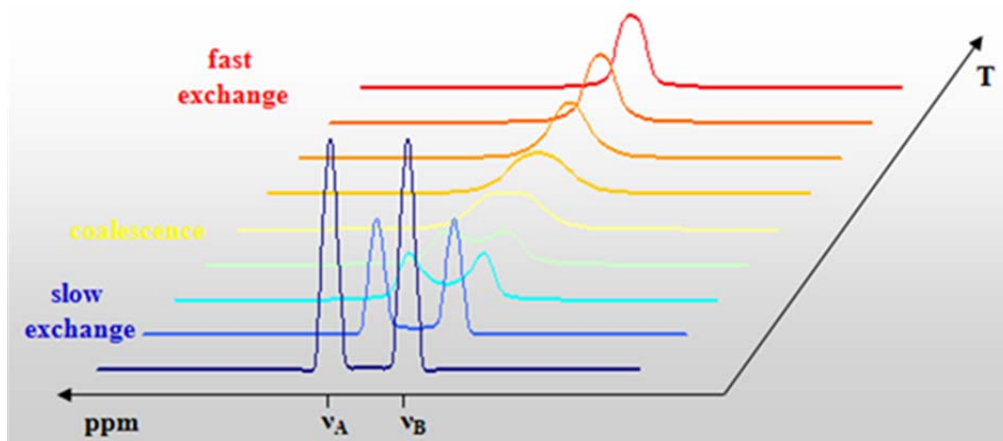
Figure 28. Evolution of two signals on raising the temperature.

As the temperature is increased, the exchange become fast with respect to the NMR timescale and lineshape gradually changes. An important point in this sequence is the so called coalescence (yellow trace) and on further increasing the temperature only a single averaged signal is observed (red trace).

The rate constants of the process can be calculated at the coalescence temperature with the equation:

$$k_{T_c} = \pi \frac{\Delta \upsilon}{\sqrt{2}}$$

The difference in the chemical shift (in Hz) of the two signals without exchange is expressed by $\Delta \upsilon$. This equation can be applied only when the two conformers are equally populated and if the signals have a sufficient separation at low temperature ($\Delta \upsilon$ is proportional to the magnetic field, in this way T_c depends upon the instrument used).

The rate constants of a conformational process (usually of first-order) are independent upon the concentration, and the corresponding k values usually cover a range of a few to a few thousands reciprocal seconds (s^{-1}). So, from the *k* values free energy of activation ($\Delta G^{\neq}$ in kcal/mol) can be extracted by means Eyring equation.[37]

$$k = \kappa \frac{k_B T}{h} \, e^{-\frac{\Delta G^{\neq}}{RT}}$$

k = constant rate (s^{-1});

T = absolute temperature (K);

h = Planck's constant (1.584·10^{-34} cal·s);

k_B = Boltzmann constant (3.2998·10^{-24} cal/K);

R = universal gas constant (1.9872 cal/K·mol);

κ = transmission coefficient (can be considered equal to 1)

Solving for $\Delta G^{\neq}$ (in kcal/mol):

$$\Delta G^{\neq} = 4.574 \cdot 10^{-3} \cdot T \cdot (\log \frac{T}{k} + 10.318)$$

The determination of the exact temperature inside the sample is crucial for the determination of the thermodynamic parameters. In fact, an error of ±2 °C in the temperature causes an error in $\Delta G^{\neq}$ of 0.1$_5$ to 0.2 kcal/mol,[38] and in it is considered the main source of errors in the DNMR approach.

Although the widespread use for the simple case, the coalescence method is not applicable to interconversion of species with different thermodynamic stability or to compounds that show intricate NMR spectra with multiple coupling patterns. In these more complicated cases, the rate constants can be inferred by NMR line shape analysis and simulation with appropriate programs that are able to simulate spectra of the first order and second order and quite complex spin system.

Once good spectral simulation is obtained at the temperature where all the dynamic processes are frozen (i.e. when k → 0), a simple change of the values of the rate constants allows to optimize the subsequent simulations at different temperatures. Corrections are needed if chemical shifts, *J* couplings and conformer ratios are also temperature-dependent. Through the visual comparison of simulated and experimentally measured spectra, the kinetic constant (*k*) is obtained at each given temperature and free energy of activation ($\Delta G^{\neq}$) can then be inferred by means of Eyring equation.

In most of conformational processes, the entropic contributions is negligible because the $\Delta G^{\neq}$ is invariant with temperature within the limits of the experimental error. At this point, the average free energy of the rotation around the considered chemical bond is determined making an arithmetical mean of the calculated ΔGs.

6.2 DFT calculations

The Density Functional Theory (DFT) is a quantum mechanical modelling method used in particular in physics and chemistry to investigate the electronic structure of many-body systems. The properties of many-electron system can be determined by using functionals.

Up to the end of the 1990s, conformational calculations of organic molecules were mainly performed by molecular mechanics (e.g. MM3,[39] MMFF[40] etc.) and semiempirical methods, for example, AM1[41] or MINDO.[42]

When the application of *ab initio* methods (HF) became available for medium-sized molecules the situation was greatly improved, although the neglecting of electron correlation was a serious limitation, partially solvable only through the employment of higher methods like MP2 that in the specific case was not an easy approach due to its computational difficulty.

Contrariwise, Density Functional Theory (DFT) has the great advantage of taking account of electronic correlation at reasonable computational cost.[43]

The basic idea of DFT is that the wavefunction and all other molecular electronic properties, for a collection of electrons and nuclei the ground state molecular energy, are uniquely determined by the electron probability density $\rho(x,y,z)$, function of three variables.

Anyway, in recent years, the availability of inexpensive high-performance servers and manageable software (Gaussian09[35] and Spartan being the most famous) has allowed high-level calculations to be performed in a reasonable amount of time for molecules containing up to DFT calculations are very interesting because they can be applied both to obtain the conformations ground states and also to find the correct geometries and energies of ground and transition states and thanks to vibrational analysis, there is always confirmation that correct transition state has been unambiguously identified.

Ground states

Some uncertainty is involved in determining the relative energies of possible ground states. In recent years many papers addressing the performance of various DFT

functionals in determining relative energies in reactions have appeared,[44] but for conformational analysis there have been very few.

For accuracy consideration the smallest basis set used is generally 6-31G* or the equivalent. Interestingly, there is only a small increase in accuracy obtained by using very large basis sets. This is probably due to the fact that the density functional has limited accuracy compared to that of the basis set. The accuracy of results from DFT calculations can be poor to fairly good, depending on the choice of basis set and density functional.

The geometries obtained by calculations can in many cases be checked by X-ray diffraction data, and the relative energies of conformations can be compared with the results of variable- temperature NMR spectroscopy. Although such a calculation usually refers to an isolated molecule, whereas X-ray studies reflect the solid state and NMR results are for solutions, DFT structures compare very well with experimental observations in almost all cases, and the relative energies of possible conformations are correctly calculated.

Transition states

Furthermore, the wavefunction approach allow DFT calculations to be used to unambiguously find the correct geometry and energy of a transition state, which is a crucial point for conformational analysis. The correct simulation of energy barriers can greatly help the understanding of dynamic processes detected by variable-temperature NMR approach.

The determination of transition state structures and energies is a crucial point for dynamic analysis, because correct simulation of energy barriers could greatly help the understanding of dynamic processes detected by dynamic NMR spectroscopy. As addressed by D. Young,[45] a transition state (or saddle point) structure is mathematically defined as "*the geometry that has zero derivative of energy with respect to moving every one of the nuclei, and has positive second derivative energy for all but one geometric movement*". In other words, a transition state linking two energy minima represents a maximum of energy in the direction of the reaction path, but it is a minimum in all other directions.

Once a stationary point is found, the primary way to verify whether it corresponds to a transition state is to compute the vibrational frequencies. A transition state must have only one negative (i.e., imaginary) frequency, and the vibrational motion associated with this frequency corresponds to the motion going towards reagents in one direction, and towards the products in the other.

Unfortunately, in contrast with the transition states for high-energy processes (such as those involved in a chemical reaction), in which the imaginary frequency usually has a large value, transition states involved in internal dynamic processes usually display small negative vibrational frequencies and can therefore be difficult to locate, especially in the presence of other possible internal motions. On the other hand, the geometry of a transition state is much simpler to idealise, because many geometrical parameters are fixed by the molecular scaffold.

6.3 X-ray diffraction (XRD)[46]

X-ray diffraction is a non-destructive technique used for the determination of the structure of crystalline systems. The structural analysis of the crystals is based on the phenomenon of X-ray diffraction.

X-ray were discovered in 1985 by Rontgen and were so named because their nature was unknown at the time. In 1912, during the study of Laue experiment, the 22 years old Bragg realized that X-rays could be used to determine the structure of the crystal and therefore to know the coordinates of the atoms contained in the unit cell. There are seven crystals systems into which all crystals can be classified (cubic, tetragonal, orthorhombic, hexagonal, rhombohedral, monoclinic, triclinic) and these systems can generate up to 230 crystallographic space groups that are identified as possible crystal symmetries.

This discovery provided a new method for investigating the fine structure of matter. For this discovery, Bragg was awarded the Nobel prize in 1915 and 40 years later he discovered that X-ray crystallography was able to reveal the double-helical structure of DNA.

In this technique the sample is irradiated by a beam of X-rays emitted from an X-ray tube and the wavelength of this beam is of the same order of magnitude of the spacing between atoms in a crystal. The physical phenomenon of diffraction by a crystal can be seen as a reflection phenomenon of the incident radiation by the planes of the crystal

lattice defined by Miller indices (h, k, l). Diffraction occurs only when there is positive interference between the electromagnetic waves reflected from the various lattice planes. And the interference will be constructive only if the path difference between the rays reflected from the contiguous levels is equal to a multiple of the wavelength, in accordance with Bragg's law:

$$n\lambda = 2dsen\theta$$

where:

n : diffraction order;

λ : wavelength of a given spectral line;

d : distance between a specific set of lattice planes;

θ : angle of incidence or diffraction of X-ray beams reflected from the crystal.

The size and the shape of the unit cell determine the angular position of the diffraction lines, and the arrangement of the atoms within the unit cell determines the relative intensities of the lines.

6.4 Electronic Circular Dichroism (ECD)

The knowledge of absolute configuration is mandatory in many industrial applications. For pharmaceutical applications, it is required that the absolute configuration of chiral drugs is known and that the biological activity of the compounds is tested for both enantiomers. Production of new drugs also requires a verification of the enantiomeric purity of the compounds. This leads to the need for characterizing their chiral purity and absolute configuration. One widely used method to detect and analyse chirality is the determination of the optical activity by circular dichroism (CD).[47] In biology, for example, electronic circular dichroism (ECD) spectra are frequently used to characterize the secondary structure of proteins. [48]

Circular dichroism (CD) is the difference in the absorption of left-handed circularly polarized light (L-CPL) and right-handed circularly polarized light (R-CPL) and occurs when a molecule contains one or more chiral chromophores (light-absorbing groups).

$$\Delta\varepsilon = \varepsilon_L - \varepsilon_R$$

CD may be regarded as one of the most powerful techniques for stereochemical analyses: it is sensitive to the absolute configuration as well as to conformational features, which are often completely obscured in the ordinary absorption spectrum.[49]

Measurements carried out in the visible and ultra-violet region of the electro-magnetic spectrum monitor electronic transitions, and, if the molecule under study contains chiral chromophores then one CPL state will be absorbed to a greater extent than the other and the CD signal over the corresponding wavelengths will be non-zero. A circular dichroism signal can be positive or negative, depending on whether L-CPL is absorbed to a greater extent than R- CPL (positive CD signal) or to a lesser extent (negative CD signal).

The CD of pure enantiomers differs in sign, but not in magnitude and there isn't simple relation between the absolute configuration of an enantiomer and the sign of its ECD spectrum. In fact, CD depends on details of the electronic and geometric molecular structure.[50]

The experimental ECD of the investigated molecule is usually displayed with the one resulting from calculated theoretical curve.

The spectra of the two enantiomers of a chiral molecule are conditioned by the chromophores in their environment. The appearance of the CD spectrum: position, intensity and sign of the bands reflect the environment of each chromophore. Therefore, the ECD spectra depend sensitively on the nature of the solvent and in some cases sign inversion was observed.

Classical force-field MD simulations constitute a possible route to explicitly account for interactions between molecule and solvent.[51] Apart from the high computational cost it might appear most desirable to treat the solute embedded in a large number of solvent molecules within a first-principles quantum mechanical MD approach. This might only be possible with very efficient electronic structure methods such as DFT which on the other hand have deficiencies for non-covalent long-range interactions.[52] Time-dependent density functional theory (TD-DFT) is presently the most widely used electronic structure method for ECD calculations. It extends the basic ideas of ground-state density-functional theory (DFT) to the treatment of excitations or more general time-dependent phenomena.

It turns out that, even with the simplest approximation to the Kohn-Sham potential, spectra calculated within this framework are in very good agreement with experimental results.[53]

7. References

[1] Smith M. B.; *March's Advanced Organic Chemistry: Reactions, Mechanisms, and Structure*, 7th edition, Cram 101, **2013**.

[2] Pasteur, L. *Ann. Chim. Physique* **1848**, *24*, 442-459.

[3] Wolf C.; *Dynamic Stereochemistry of Chiral Compounds*, RSC Publishing, **2008**.

[4] a) Ho, T.-L. Stereoselectivity in Synthesis, Wiley-VCH, New York, **1999** b) Lin, G.-Q.; Li, Y.-M.; Chan A. S. C. *Principles and Applications of Asymmetric Synthesis*, Wiley-VCH, New York, **2001**.

[5] a) Ojima, I. *Catalytic Asymmetric Synthesis*, 2nd edition, Wiley VCH, New York, 2000 b) Noyori, R. *Angew. Chem., Int. Ed.* **2002**, 41, 2008-2022.

[6] Reist, M.; Carrupt, P.-A.; Francotte, E.; Testa, B.; *Chem. Res. Toxicol.*, **1998**, *11*, 1521-1528.

[7] Kuhn, R. *Stereochemie* Frendenberg, K. Ed. Deutike, F. **1933**, 803.

[8] Kottas, G. S.; Clarke, L. I.; Horinek, D.; Michl, J.; *Chem. Rev.* **2005**, *105*, 1281−1376.

[9] Oki, M.*Topics in Stereochemistry,* **1983**.

[10] a) Clayden, J.; Moran, W. J.; Edwards ,P. J.; LaPlante, S. R.; *Angew. Chem. Int. Ed.* **2009**, *48*, 6398–6401 b) LaPlante, S. R.; Fader, L. D.; Fandrick, K. R.; Fandrick, D. R.; Hucke, O.; Kemper, R.; Miller, S. P. F.; Edwards, P. J. *J. Med. Chem.* **2011**, *54*, 7005–7022 c) LaPlante, S. R.; Edwards, P. J.; Fader, L. D.; Jakalian, A.; Hucke, O.; *ChemMedChem* **2011**, *6*, 505 – 513.

[11] Bringmann, G.; Mortimer, P. A. J.; Keller, P. A.; Gresser, M. J.; Garner, J.; Breuning, M.; *Angew. Chem. Int. Ed.*, **2005**, *44*, 5384.

[12] a) Bringmann, G.; Menche, D.; Kraus, J.; Mühlbacher, J.; Peters, K.; Peters, E. M.; Brun, R.; Bezabih, M.; Abegaz, B. M. *J. Org. Chem.* **2002**, *67*, 5595-5610. b) Kuroda, M.; Mimaki, Y.; Sakagami, H.; Sashida, Y. *J. Nat. Prod.* **2003**, *66*, 894-897.

[13] a) Wang, X.; Howell, C. P.; Chen, F.; Yin, J.; Jiang, Y.; Gossypol—a polyphenolic compound from cotton plant. *Adv Food Nutr Res*. **2009**, *58*, 215-263 b) Coutinho EM. Gossypol: a contraceptive for men. Contraception **2002**, *65* (4), 259-263.

[14] a) Lipscomb, W. N.; Angew. Chem. 1977, 89, 685-696 b) Brown, H. C.; Angew. Chem. 1980, 92, 675-683 c) Suzuki, A.; *Angew. Chem.* **2011**, *123*, 6854-6869 ; *Angew. Chem. Int. Ed.* **2011**, *50*, 6722-6737.

[15] Baker, S. J.; Tomsho, J. W.; Benkovic, S. J.; *Chem. Soc. Rev.* **2011***, 40,* 4279-4285.

[16] Campbell, P. G.; Marwitz, A. J. V.; Liu, S.-Y.; *Angew. Chem. Int. Ed.* **2012**, *51*, 6074-6092.

[17] Dewar, M. J. S.; Kubba, V. P.; Pettit, R.; *J. Chem. Soc*. **1958**, 3073-3076.

[18] Dewar, M. J. S.; R. Dietz, *J. Chem. Soc*. **1959**, 2728-2730.

[19] a) Campbell, P.G.; Marwitz, A. J.V.; Liu, S.-Y. *Angew. Chem. Int. Ed.* **2012**, *51*, 6074; b) Bosdet, M.J.D.; Piers, W.E. *Can. J. Chem.* **2009**, *87*, 8. a) Liu, Z.; Marder, T.B. *Angew. Chem. Int. Ed.* **2008**, *47*, 242.

[20] a) Marwitz, A. J. V; Matus, M. H.; Zakharov, L. N.; Dixon, D.A.; Liu, S.-Y. *Angew Chem.* **2009**, *48*, 973. b) Campbell, P. G.; Abbey, E. R.; Neiner, D.; Grant, D. J.; Dixon, D. A.; Liu, S.-Y. *J. Am. Chem. Soc.* **2010**, *132*, 18048. C) Abbey, E. R.; Zakharov, L. N.; Liu, S.-Y. *J. Am. Chem. Soc*. **2008**, *130*, 7520.

[21] C. Baldock, Gert-Jan de Boer, J. B. Rafferty, A. R. Stuitje and D. W. Rice, Biochemical Pharmacology, 1998, Vol. 55, pp. 1541–1549.

[22] a) Kervyn, S.; Fenwick, O.; Di Stasio, F.; Shin, Y. S.; Wouters, J.; Accorsi, G.; Osella, S.; Beljonne, D.; Cacialli, F.; Bonifazi, D. Chem.-Eur. J. 2013, 19,7771. b) Wang, X.-Y.; Lin, H.-R.; Lei, T.; Yang, D.-C.; Zhuang, F.-D-; Wang, J.-Y.; Yuan, S.-C.; Pei, J. Angew. Chem. Int. Ed. 2013, 52, 3117. c) Kwong, R. C.; Ma, B.; Tsai, J.-Y.; Beers, S.; Barron, E.; Kottas, G.; Dyatkin, A. B. Metal Complexes with Boron-Nitrogen Heterocycle Containing Ligands for Use in Organic Light Emitting Diodes. WO2010/ 135519 A1, Nov 25, 2010 d) Lepeltier, M.; Lukoyanova, O.; Jacobson, A.; Jeeva, S.; Perepichka, D. F. Chem Commun. 2010, 46, 7007.

[23] Bosdet, M. J. D.; Jaska, C. A.; Piers, W. E.; Sorensen, T. S.; Parvez, M. *Org. Lett.* **2007**, *9*, 1395.

[24] X.-Y. Wang; H. R. Lin; T. Lei; D.-C. Yang; F.-D. Zhuang; J.-Y- Wang; S.-C. Yuan; J. Pei *Angew. Chem. Int. Ed.* **2013**, *52*, 3117.

[25] G. Li, Y. Zhao, J. Li, J. Cao, J. Zhu, X. W. Sun, Q. Zhang, *J. Org. Chem.* **2015**, *80*, 196-203.

[26] Steven R. Wisniewski, Courtney L. Guenther, O. Andreea Argintaru and Gary A. Molander *J. Org. Chem.* **2014**, *79*, 365-378.

[27] Hatakeyama, T.; Hashimoto, S.; Seki, S.; Nakamura, M.; *J. Am. Chem. Soc.* **2011**, *133*, 18614-18617.

[28] Dewar, M. J. S.; Dietz, R. *J. Chem. Soc.* **1959**, 2728-2730.

[29] Yanai, T.; Tew, D. P.; Handy C. N.; *Chemical Physics Letters* **2004**, *393*, 51 – 57.

[30] Siegel, J. S.; Anet, F.A.L. *J. Org. Chem.* **1998**, *53*, 2629-2630.

[31] Brown, J. H.; Brushweller, C.H. DNMR6: *Calculation of NMR Spectra Subject to the Effects of Chemical Exchange (program 633)* QCPE Bulletin, Bloomington, Indiana **1983**, *3*, 103-103. A copy of the program is available on request from the authors.

[32] Eyring H. *Chem. Rev.* **1935**, *17*, 65-77.

[33] Casarini, D.; Lunazzi, L.; Mazzanti, A. *Eur. J. Org. Chem.* **2010**, 2035-2056.

[34] ComputeVOA 0.1: Software package for conformational calculation, integrated with Gaussian09. www.btools.com/products.html/#software

[35] Gaussian 09, rev D.01. Frisch, M. J.; Trucks, G. W.; Schlegel, H. B.; Scuseria, G. E.; Robb, M. A.; Cheeseman, J. R.; Scalmani, G.; Barone, V.; Mennucci, B.; Petersson, G. A.; Nakatsuji, H.; Caricato, M.; Li, X.; Hratchian, H. P.; Izmaylov, A. F.; Bloino, J.; Zheng, G.; Sonnenberg, J. L.; Hada, M.; Ehara, M.; Toyota, K.; Fukuda, R.; Hasegawa, J.; Ishida, M.; Nakajima, T.; Honda, Y.; Kitao, O.; Nakai, H.; Vreven, T.; Montgomery, Jr., J. A.; Peralta, J. E.; Ogliaro, F.; Bearpark, M.; Heyd, J. J.; Brothers, E.; Kudin, K. N.; Staroverov, V. N.; Kobayashi, R.; Normand, J.; Raghavachari, K.; Rendell, A.; Burant, J. C.; Iyengar, S. S.; Tomasi, J.; Cossi, M.; Rega, N.; Millam, N. J.; Klene, M.; Knox, J. E.; Cross, J. B.; Bakken, V.; Adamo, C.; Jaramillo, J.; Gomperts, R.; Stratmann, R. E.; Yazyev, O.; Austin, A. J.; Cammi, R.; Pomelli, C.; Ochterski, J. W.; Martin, R. L.; Morokuma, K.; Zakrzewski, V. G.; Voth, G. A.; Salvador, P.; Dannenberg, J. J.; Dapprich, S.; Daniels, A. D.; Farkas, O.; Foresman, J. B.; Ortiz, J. V.; Cioslowski, J.; Fox, D. J. Gaussian, Inc., Wallingford CT, **2009**.

[36] Package GaussView 5.0.9, Gaussian Inc., Wallingford CT, **2009**.

[37] Eyring, H. *Chem. Revs.* **1935**, *17*, 65.

[38] Bonini, B. F.; Grossi, L.; Lunazzi, L.; Macciantelli D. *J. Org. Chem.* **1986**, *51*, 517-522.

[39] Allinger, N. L.; Yuh, Y. H.; Lii, J.-H. *J. Am Chem. Soc.* **1989**, *111*, 8551-8566.

[40] Halgren, T. A. *J. Comput. Chem.* **1996**, *17*, 520-552.

[41] Dewar, M. J. S.; Zoebisch, E. G.; Healy, E. F.; Stewart, J. J. P. *J. Am. Chem. Soc.* **1985**, *107*, 3902-3909.

[42] Bingham, R. C.; Dewar, M J. S.; Lo, D. H. *J. Am. Chem. Soc.* **1975**, *97*, 1285-1293.

[43] Koch, W.; Houlthausen, M. C. *A Chemist's Guide to Density Functional Theory*, Wiley-VCH, Weinheim, 2nd ed., **2002**; *A primer in Density Functional Theory* (Eds.: Fiolhais, C.; Nogueira, F.; Marques, M.) Springer-Verlag, Heidelberg, **2003**.

[44] a) Check, C. E.; Gilbert, T. M. *J. Org. Chem.* **2005**, *70*, 9828– 9834; b) Wodrich, M. D.; Corminbouef, C.; Schleyer, P. v. R. *Org. Lett.* **2006**, *8*, 3631–3634; c) Shreiner, P. R.; Fokin, A. A.; Pascal, R. A.; De Mejere, A. *Org. Lett.* **2006**, *8*, 3635–3638; d) Grimme, S. *Angew. Chem. Int. Ed.* **2006**, *45*, 4460–4464; e) Zhao, Y.; Truhlar, D. G. *Org. Lett.* **2006**, *8*, 5753–5755; f) Rokob, T. A.; Hamza, A.; Pápai, I. *Org. Lett.* **2007**, *9*, 4279–4282; g) Shreiner, P. R. *Angew. Chem. Int. Ed.* **2007**, *46*, 4217–4219; h) Wodrich, M. D.; Wannere, C. S.; Mo, Y.; Jarowski, P. D.; Houk, K. N.; Schleyer, P. v. R. *Chem. Eur. J.* **2007**, *13*, 7731–7744; i) Zhao, Y.; Truhlar, D. G. *Acc. Chem. Res.* **2008**, *41*, 157–167; j) Schwabe, T.; Grimme, S. *Acc. Chem. Res.* **2008**, *41*, 569–579; k) Wodrich, M. D.; Jana, D. F.; Schleyer, P. v. R.; Corminbouef, C. *J. Phys. Chem. A* **2008**, *112*, 11495–11500.

[45] Young, D. *Computational Chemistry*, chapter 17, pp. 147– 158, Wiley Interscience, New York, **2001.**

[46] Warren, B. E.; *X-Ray Diffraction*, Addison-Wesley, Reading, MA, **1969.**

[47] Berova, N.; Nakanishi, K.; Woody, R. W. *Circular dichroism, Principles and applications*, 2nd Edition, Wiley-VCH, **2000.**

[48] a) Fasman GD. *Circular Dichroism and the Conformational Analysis of Biomolecules*. New York: Plenum Press; **1996**. b) Manavalan, P; Johnson, W.C. *J Biosci* **1985**, *8*, 141–149. c) Sreerama, N; Venyaminov, SY; Woody, RW. *Anal Biochem* **2000**, *287*, 243–251.

[49] Berova, N; Di Bari, L.; Pescitelli, G. *Chem. Soc. Rev.* **2007**, *36*, 914-931.

[50] Warnke, I.; Furche, F. *WIREs Comput Mol Sci* **2012**, *2*, 150-166.

[51] a) Kundrat, M. D.; Autschbach, J. *J Chem Theory Comput* **2009**, *5*, 1051–1060. b) Mukhopadhyay, P.; Zuber, G.; Goldsmith, M.; Wipf, P.; Beratan, D.N. *Chem Phys Chem* **2006**, *7*, 2483–2486. c) Bernasconi, L.; Blumberger, J.; Sprik, M.; Vuilleumier, R. *J Chem Phys* **2004**, *121*, 11885–11899

[52] Autschbach, J. *Chirality* **2009**, *21*, E116– E152.

[53] Marques, M. A. L.; Gross, E. K. U. *Time-dependent Density Functional Th*eory